Chapter 6

Building Response Prediction

This chapter interprets the simulated building responses by developing relationships to predict collapse, the permanent total drift ratio, and peak inter-story drift ratio (IDR) from ground motion intensity measures. Previous chapters consider the simulation results for each ground motion study individually. In that light, the results describe regional patterns of building response. The building response prediction models developed in this chapter disregard which study produced the ground motions and consider only the building response as a function of intensity measure. Since these prediction models include a measure of the uncertainty due to nonlinearities in building response, it is reasonable to forgo the full nonlinear time history analysis for some purposes. These relationships can be used as general structural analyses to approximate the lifetime costs of a proposed steel moment-resisting frame (MRF) design, or to compare at an initial stage several designs, or for other general analyses.

6.1 Simulated Ground Motions and Ground Motion Prediction Equations

Simulated earthquakes of magnitudes 6.3–7.8 produced the ground motions used in this thesis. The sites of the ground motions range from 1 to 200 km distant to the generating fault. Figure 6.1 compares the magnitudes of the simulated earthquakes to the measure of distance between the faults and ground motion sites for all simulation do-

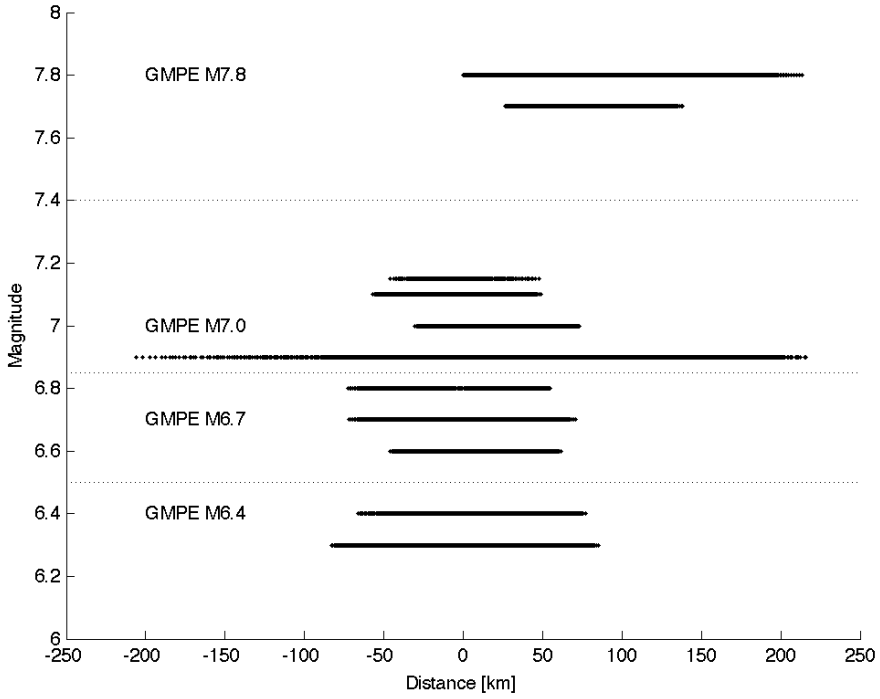

Figure 6.1: The simulated ground motions in this thesis cover a range of magnitudes and distances between the fault and ground motion site. Negative distances are sites on the hanging wall of a thrust fault. This figure shows the magnitude grouping of the simulations for comparison with ground motion prediction equations.

mains. This distance is the shortest path between each site and the surface projection of the rupture on a strike-slip fault or the projection of the top edge of a thrust fault. Figure 6.2 shows the peak ground displacements (PGD_{lp}s) and peak ground velocities (PGV_{lp}s) of the simulated ground motions as functions of the distance between the fault and the site. Since there are not many recorded ground motions within 10 km of a large magnitude earthquake, these simulated ground motions suggest what the peak ground displacements and velocities may be for near-source records of strong ground motions.

Figure 6.3 compares the simulated ground motions to the extended magnitude ground motion prediction equations (GMPEs) by Cua and Heaton (2008). For the smallest simulations (magnitudes 6.3 and 6.4), the GMPEs and the simulated ground motions do not agree. At rock and soil sites within 5 km of the fault, the median

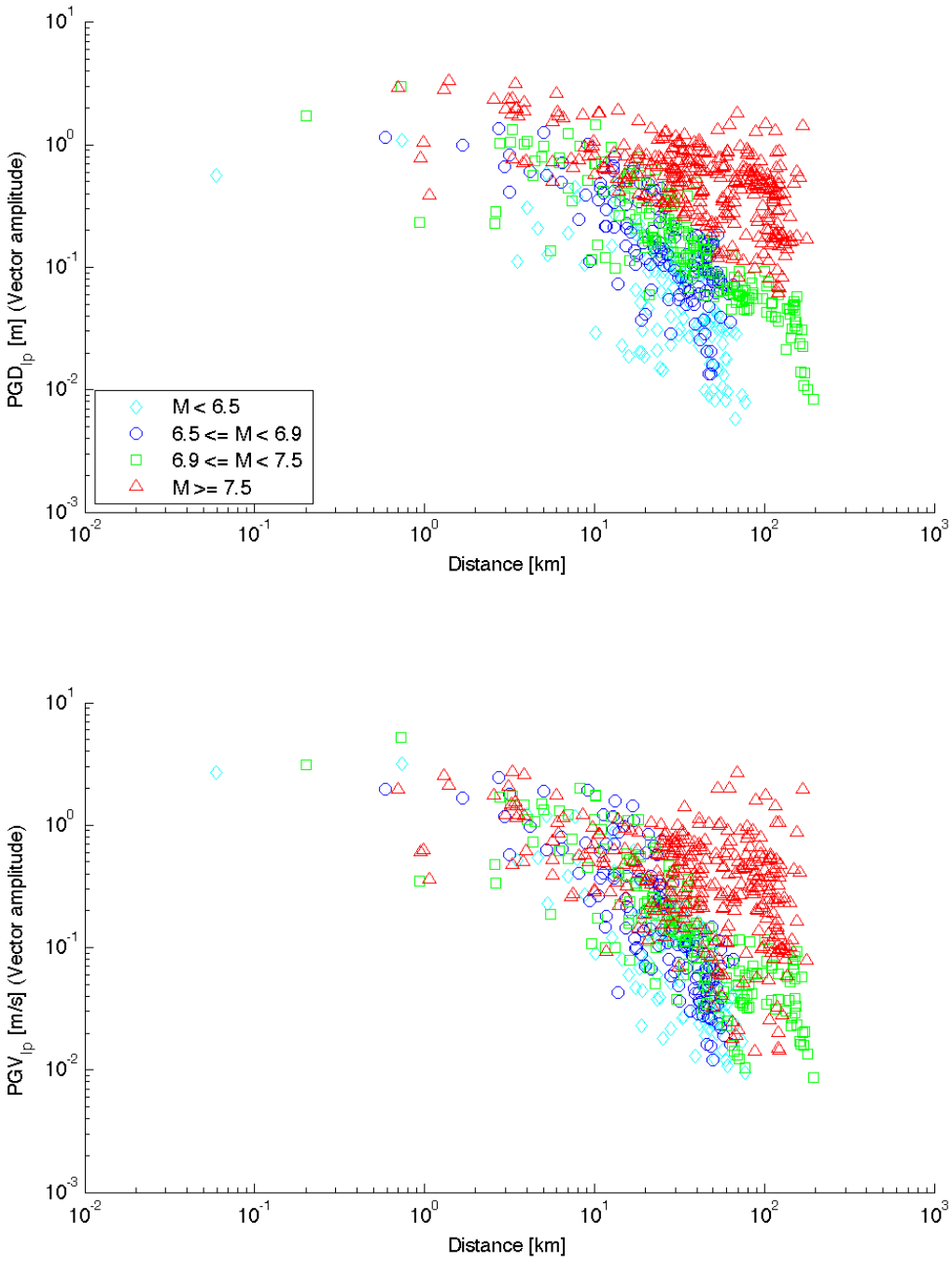

Figure 6.2: There are few recorded ground motions from near-source sites in strong ground motions. The simulated ground motions in this thesis suggest what the long-period peak ground displacements and velocities may be for near-source sites.

PGV_{lp} of the simulated ground motions is more than one log-standard deviation from the GMPE median PGV. The GMPE median PGV saturates at small distances whereas the median PGV_{lp} of the simulated ground motions continues to increase linearly on the log-scale. For the large simulations (magnitudes 6.6 to 7.2), the GMPE and simulated ground motions generally agree for rock sites but not for soil sites. At soil sites within 10 km of the fault, the median PGV_{lp} of the simulated ground motion is more than one log-standard deviation from the GMPE median PGV. For the largest magnitudes (7.7 and 7.8), the median PGV_{lp} of the simulated ground motions is generally within one log-standard deviation of the predicted median. However, the median PGV_{lp} of the simulated ground motions at sites within 10 km are consistently larger than what is predicted.

For sites 30 to 200 km distant from the rupture of the largest magnitude earthquakes, the log-standard deviation of the simulated ground motions can be twice that of the GMPEs. Figure 6.4 shows the data that produced these large log-standard deviations. The large spread is consistent for the three sets of southern San Andreas simulations. (Although, TeraShake 1 has some unusually small peak ground velocities.) The spread in the peak ground velocity from the simulations based on the 1906 San Francisco earthquake on the northern San Andreas fault is smaller than the spread from the southern San Andreas events. Thus the southern San Andreas ground motions are the source of the unexpectedly large uncertainty in peak ground velocity for distant sites in the largest magnitude earthquakes.

For the building response prediction models developed in the following sections to be widely applicable, they must be based on plausible ground motions. The simulated ground motions used to calculate the steel MRF responses should be reasonably consistent with the patterns of recorded ground motions. The simulations and empirical relations need not match exactly because there are gaps in the recorded data and the building response prediction models disregard the magnitude and distance information associated with each ground motion. Each study that produced the simulated ground motions used in this thesis was satisfied that the ground motions were plausible. (The TeraShake 2 simulations are now considered more likely than TeraShake 1

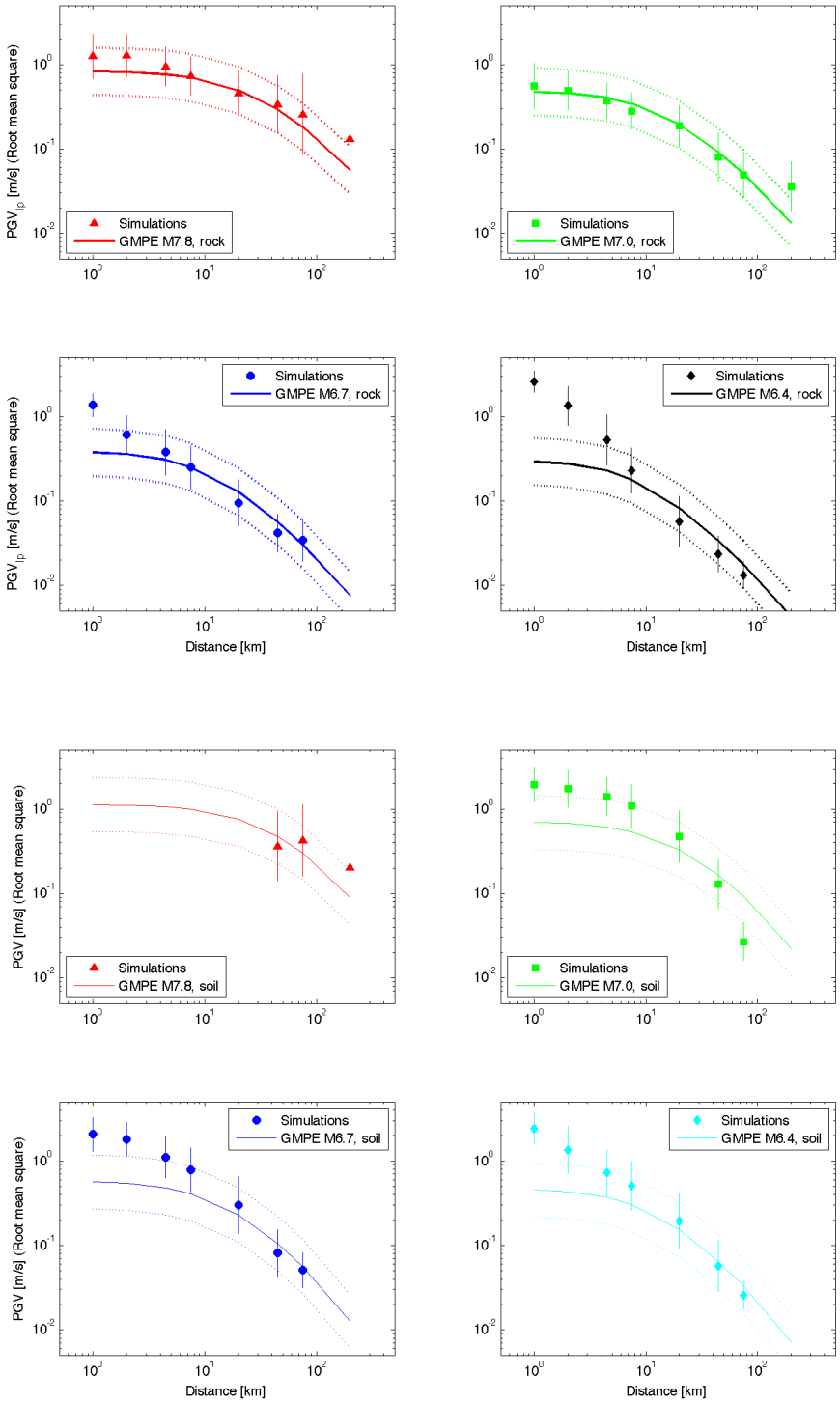

Figure 6.3: This figure compares the peak ground velocity medians and log-standard deviations of the simulated ground motions to those of GMPEs by Cua and Heaton (2008). The top four plots compare rock sites (shear wave speeds greater than 464 m/s), and the bottom four plots compare soil sites (shear wave speeds less than or equal to 464 m/s). Each plot compares PGVs from similar magnitudes; Figure 6.1 defines the magnitude groups. Note that the long-period PGVs have been converted to the root mean square velocity: $\mathrm{PGV_{rms}} = \mathrm{PGV_{lp}}/1.18$ (Cua and Heaton, 2008). Converting long-period, vector amplitude PGV to broadband, vector amplitude PGV does not significantly affect this comparison.

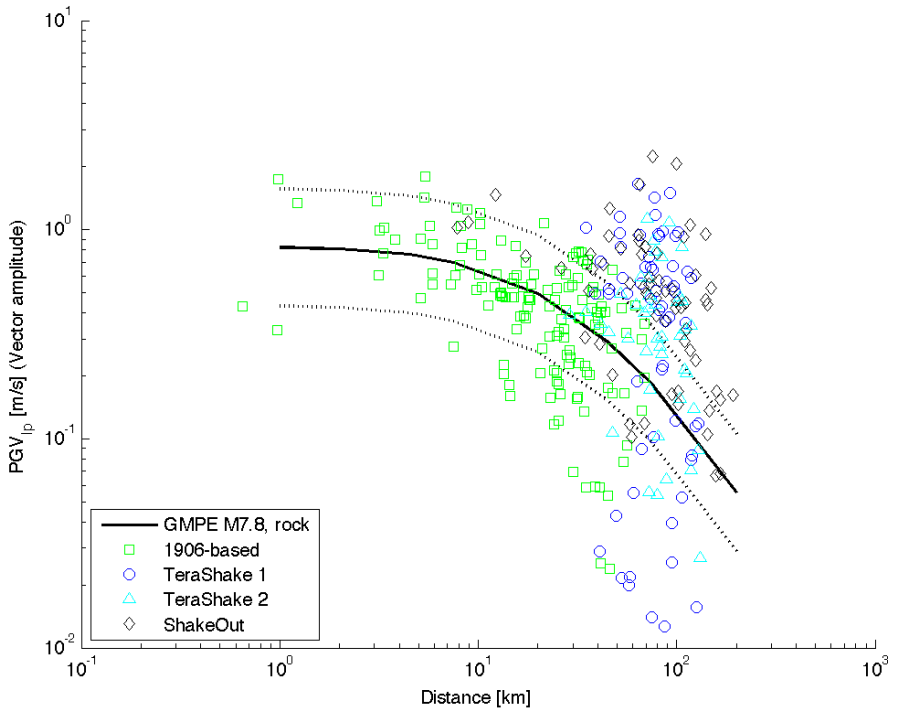

Figure 6.4: This figure shows the long-period peak ground velocities for the largest magnitude simulations at rock and soil sites. The data for sites over 30 km from the fault have a large spread. The simulations on the southern San Andreas (TeraShake and ShakeOut) contribute exclusively to the large range of peak ground velocities at distant sites.

because its less coherent source model generated ground motions more consistent with past experience and current expectations.) With further investigation, seismologists may reconcile the differences between the simulated ground motions and the GMPEs. The simulated ground motions are sufficiently consistent with the expectations developed from recorded ground motions to justify their use in developing building response prediction models.

6.2 Bayesian Model Class Selection

This section develops models to predict the state of a steel MRF building from intensity measures of ground motions. The states of building response are: collapsed or standing; total structural loss or repairable; and if repairable, the peak IDR. I propose several possible prediction models and apply Bayesian model class selection to determine the most likely prediction model based on the simulated building responses, the structure of the proposed model, and prior information about the parameters of the models.

6.2.1 Data

The intent of this thesis is to model steel moment frame building response in strong ground motions. Building responses in small ground motions can be adequately modeled by modal analysis because the buildings remain elastic. Approximately one-third of the simulated ground motions in this thesis can be considered too small to induce inelastic building behavior. These small ground motions would dominate the fit of the building response prediction models. Thus, I remove data for PGD_{lp} less than 0.15 m and PGV_{lp} less than 0.3 m/s. Removing these ground motions from the data set results in prediction models that better describe building response in strong ground motions. Figure 6.5 locates the remaining data in the PGD_{lp}-PGV_{lp} plane and indicates the amount of data at each location. The preponderance of the data is from ground motions with PGD_{lp} less than 1.5 m and PGV_{lp} less than 1.5 m/s.

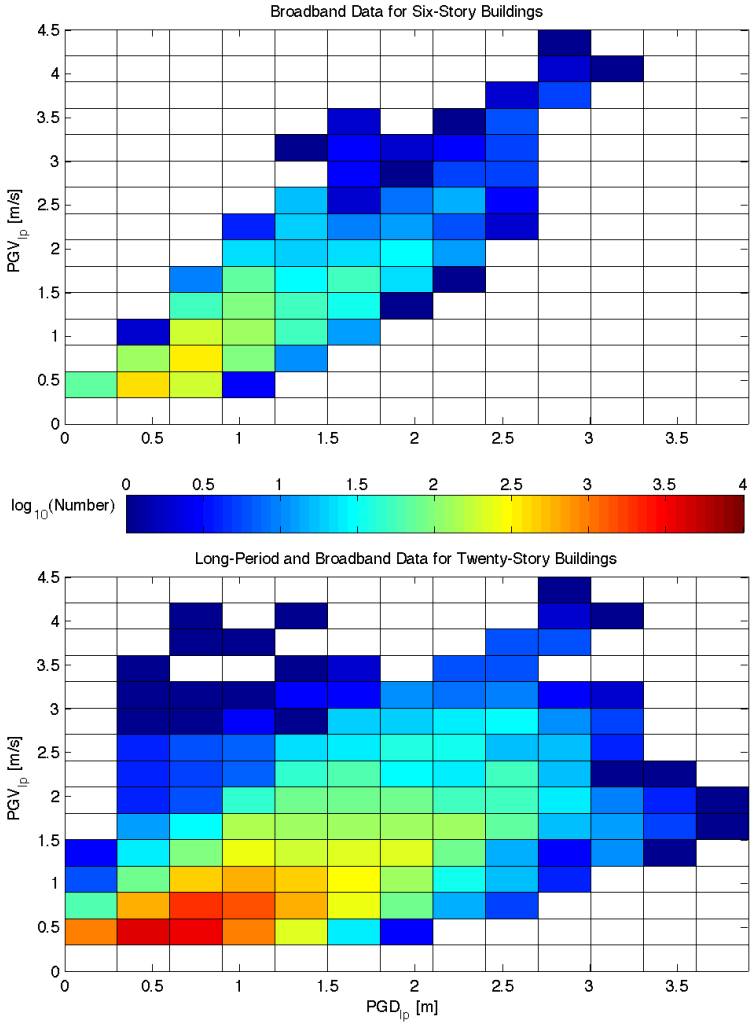

Figure 6.5: This figure shows the location of data in the PGD_{lp}-PGV_{lp} plane. Ground motions with PGD_{lp} less than 0.15 m and PGV_{lp} less than 0.3 m/s have been removed. The remaining data comes primarily from ground motions with PGD_{lp} less than 1.5 m and PGV_{lp} less than 1.5 m/s.

The data set for the six-story buildings is different than that for the twenty-story buildings. Approximately 10% of the ground motions are broadband, which can be applied to both six- and twenty-story building models. Most simulated ground motions in this thesis are long-period, which can only be applied to the twenty-story buildings. Furthermore, the peak ground measures of broadband ground motions are almost always larger than those of long-period ground motions. I apply a low-pass Butterworth filter with a corner period of 2 s to the broadband ground motions in order to make the peak ground measures consistent. I filter the broadband ground motions only to produce consistent PGD and PGV measures; the nonlinear time history analyses use the unfiltered simulated ground motions. Thus, the PGD and PGV in this chapter are calculated from long-period ground motions.

The peak ground displacements and velocities of the data set for the six-story buildings are highly correlated, whereas the data set for the twenty-story buildings does not show a strong correlation. The prediction models for the six-story buildings should only be applied to ground motions with a PGD approximately equal to the PGV. The prediction models for the twenty-story buildings can be applied to ground motions in a larger area of the PGD-PGV plane.

The building responses as a function of PGD and PGV are consistent with intuition: larger PGDs and PGVs induce larger building responses (Figures 6.6–6.8). Generally speaking, the six- and twenty-story models with perfect welds collapse in ground motions with PGD_{lp} greater than 1 m and PGV_{lp} greater than 2 m/s (Figure 6.6). Models with brittle welds collapse in smaller ground motions than do models with perfect welds. For ground motions with PGD_{lp} greater than 0.6 m and PGV_{lp} greater than 0.6 m/s, the building may remain standing but be deemed a total structural loss (defined in this thesis as a permanent total drift ratio greater than 0.0091; Figure 6.7). In many simulations with large ground motions, the buildings experience large dynamic inter-story drifts but are not total structural losses (Figure 6.8).

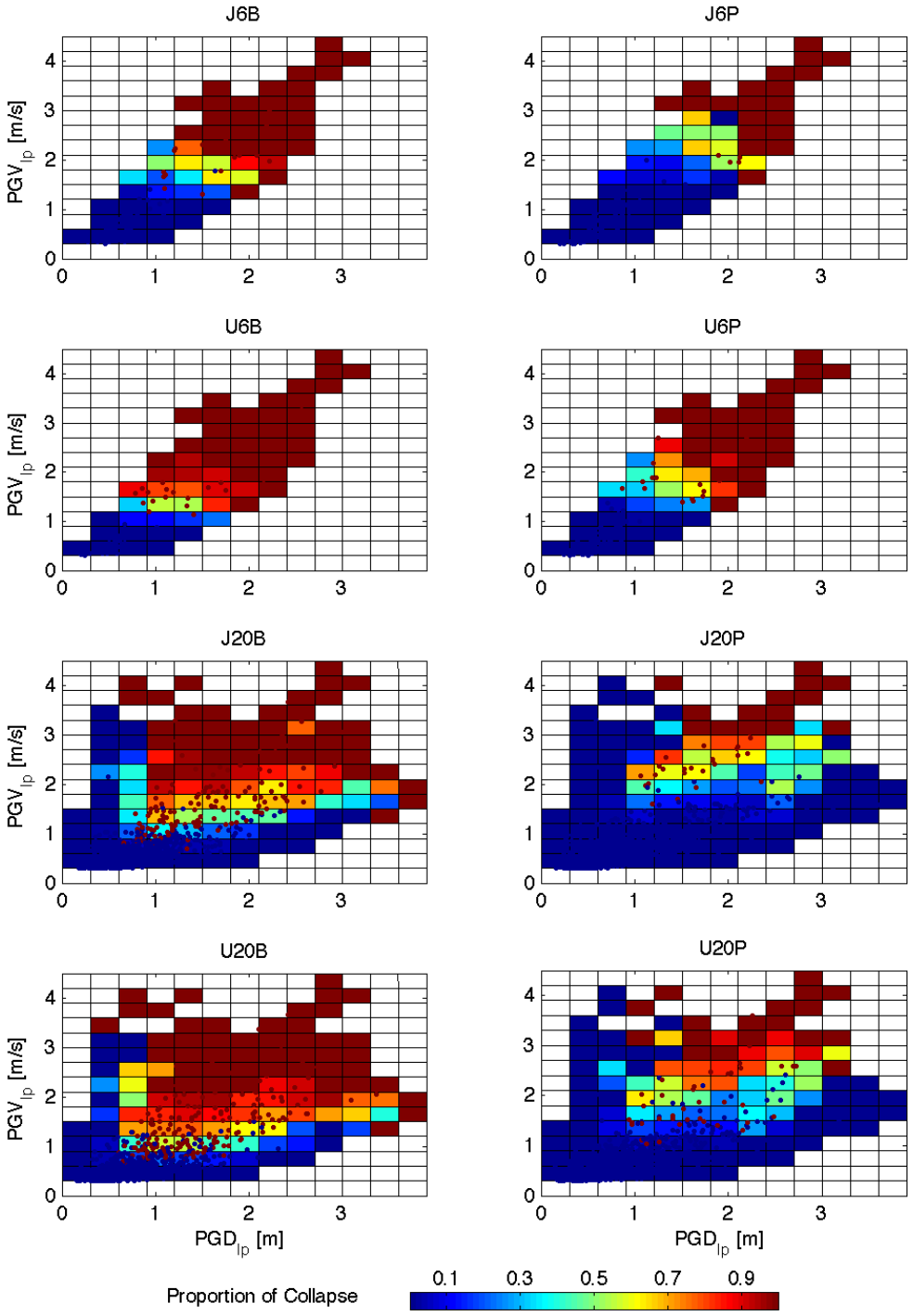

Figure 6.6: This figure shows the location of collapse data in the PGD_{lp}-PGV_{lp} plane. The coloring of a box represents the proportion of buildings that collapse in that range of PGD_{lp} and PGV_{lp}. Blue and red dots locate some data points for buildings that remain standing or collapse, respectively.

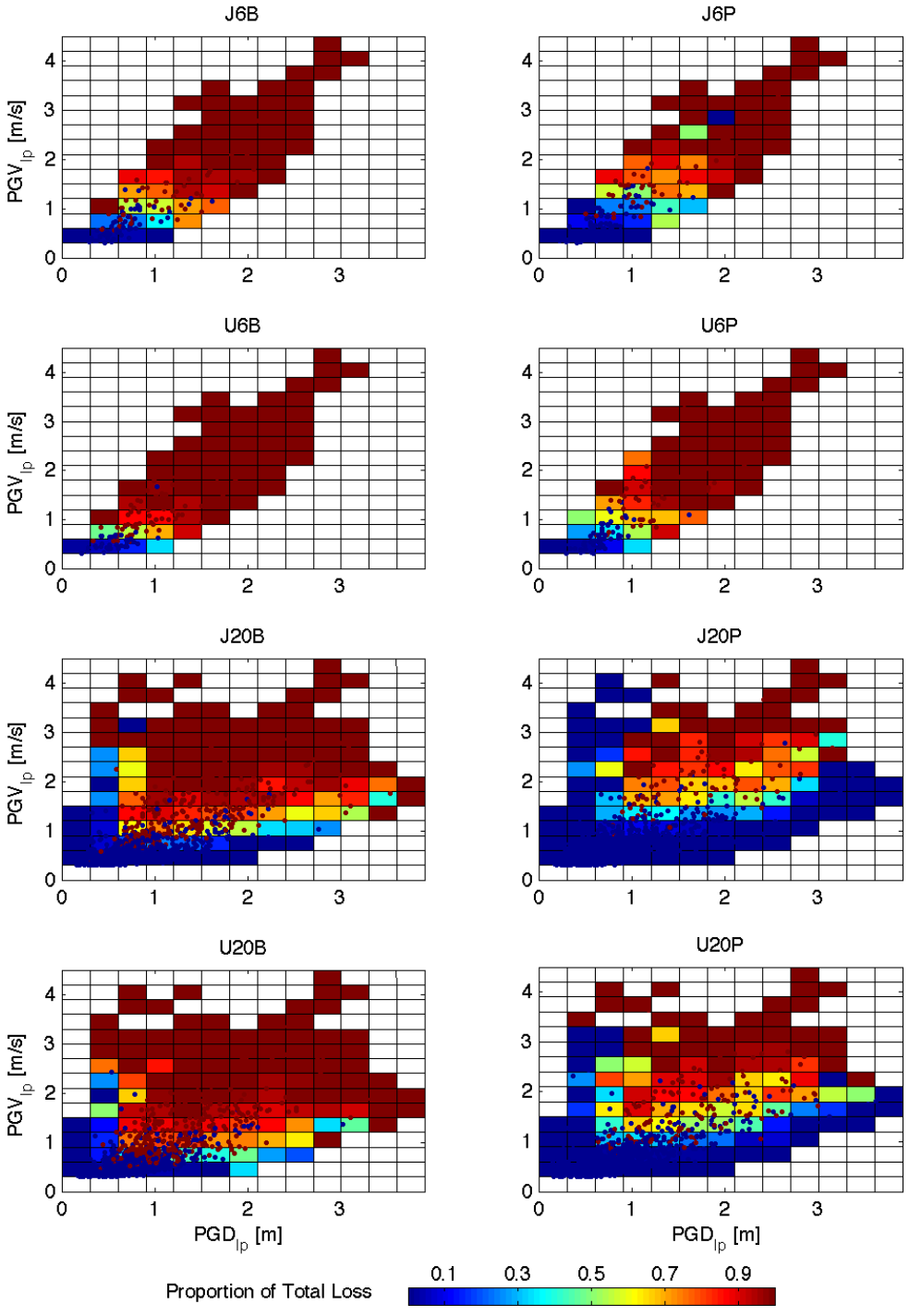

Figure 6.7: This figure locates the total structural loss data in the PGD_{lp}-PGV_{lp} plane. Similar to the plot of collapse data, the box color represents the proportion of buildings that are a total structural loss, and blue and red dots locate some data points for buildings that are repairable or a total structural loss, respectively.

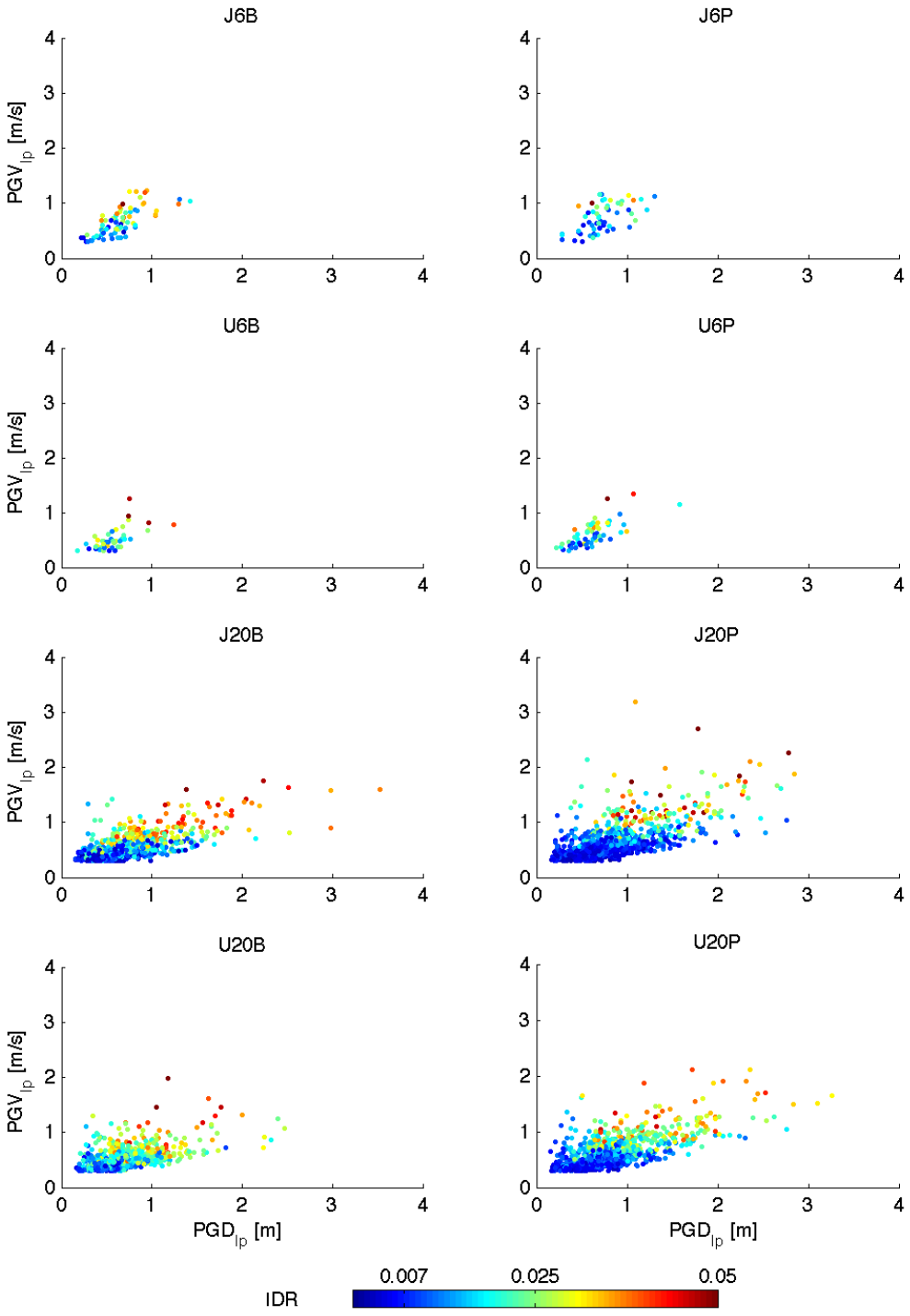

Figure 6.8: This figure locates some of the peak IDR data in the PGD_{lp}-PGV_{lp} plane. The color of the data indicate the peak IDR. The peak IDR data assumes that the building is not a total structural loss.

6.2.2 Theory

Bayesian model class selection is a technique to compare proposed models based on the Bayesian interpretation of probability and statistics. The fundamental distinction between the traditional, or frequentist, and Bayesian approaches is the understanding of probabilistic statements. (See, for example, Gill (2002) or Muto (2006).) A frequentist understands probability as the long-term outcome of repeated trials; a Bayesian understands probability as a degree of belief, or degree of plausibility, which may be different for different observers. For this thesis, an important consequence of the Bayesian approach is the treatment of uncertain model parameters. Traditional model fitting determines values for uncertain model parameters by minimizing the least squares error, and an ad hoc information criterion can be used to compare proposed models. Bayesian model fitting uses a probability density function (PDF) of the uncertain model parameters to represent the plausibility of different parameter value combinations. Analysis of this PDF (that is, its maximum and average values) determines the most probable model among the proposed models based on prior information, or judgement, and available data.

There are two levels of analysis in Bayesian model class selection: (1) determine the most probable values of the uncertain parameters for each proposed model class; and then (2) determine the most probable model class from the proposed model classes. A model class refers to the general structure of a proposed model with N_B uncertain parameters. The uncertain parameters form a N_B-dimensional space (also known as the parameter space). A particular combination of the parameter values defines a particular model in the model class. A PDF in the parameter space quantifies the relative likelihood of each combination of parameter values based on available information. For example, previous studies may suggest a model class, and there is data which can revise, or update, the parameter values. In this case, the PDF quantifies both the prior information and the new data. If there were no previous studies, then the PDF would only quantify the information in the new data. The PDF is used to determine the most probable values of the uncertain parameters, as

well as the most probable model class.

The posterior PDF updates prior information about the uncertain parameter values with information from collected data using Bayes' Theorem. Mathematically, the posterior PDF is proportional to the product of the prior PDF and the likelihood function (Equation 6.1, lines 1 and 2). The prior PDF is a weighting function over the parameter space based on judgement from prior information. For example, a model with negative parameter values may be undefined, and therefore the prior PDF would be zero where the parameter values are negative. In another application, previous studies may recommend certain combinations of parameter values (here the prior PDF may be assigned a higher value), and thus significantly different combinations of parameter values are not expected (here the prior PDF may be assigned a lower value). The likelihood function quantifies the probability of observing the available data set from the model defined by a particular combination of the parameter values (line 3 of Equation 6.1). In other words, assuming only a model defined by a particular combination of parameter values (for example, β_1 for model class $\mathcal{M}_1$), the likelihood function at β_1 is the probability of getting all the available data according to that model. The likelihood function at another combination of parameter values (say, β_2) is the probability of getting the same available data according to this second model in model class $\mathcal{M}_1$. In this way, each model class has an associated posterior PDF constructed from prior information and the available data, through Bayes' Theorem as follows:

$$
\begin{aligned}
\text{Posterior PDF} &\propto \text{(prior PDF)(likelihood function)} \\
p(\beta \,|\, \mathcal{D}, \mathcal{M}) &\propto p(\beta \,|\, \mathcal{M})\, p(\mathcal{D} \,|\, \beta, \mathcal{M}) \\
&\propto p(\beta \,|\, \mathcal{M}) \prod_{i=1}^{N} p(y_i \,|\, x_i, \beta, \mathcal{M}) \qquad (6.1) \\
&\quad \text{(assuming the data are independent and identically distributed)} \\
&\quad \text{where } \beta \text{ is a vector of the uncertain parameters with } N_B \text{ elements,} \\
&\quad \mathcal{D} \text{ is the set of } x_i, y_i \text{ data with } N \text{ elements,}
\end{aligned}
$$

and $\mathcal{M}$ is a proposed model class.

Each posterior PDF is a function over the parameter space, so it can be imagined as a surface over this space. A peak in the posterior PDF at β is caused by a large amount of data well modeled by the proposed model with parameter values of β. This surface can have multiple peaks, and each peak can be narrow or broad depending on the uncertainty in the parameter value. A narrow peak has less uncertainty in the parameter value, whereas a broad peak has more. The parameter values that correspond to the global maximum value of this surface are the most probable combination of parameter values for the proposed model class (Equation 6.2). Thus the most probable values of each proposed model's uncertain parameters can be found by maximizing each posterior PDF with respect to the parameters.

$$\hat{\beta} = \arg \max_{\beta \in B} p(\beta \,|\, \mathcal{D}, \mathcal{M}) \tag{6.2}$$

where $\hat{\beta}$ is the most probable combination of parameter values and B is the parameter space.

Take the linear model class $y(x) = \alpha x + \gamma$, with uncertain parameters α and γ, as an example. The set of all possible values of α and γ form a two-dimensional parameter space for this model class. A previous study suggested $\alpha \approx 6$ and $\gamma \approx 0.1$, and so the prior PDF could be quantified such that α and γ are normally distributed with means of 6 and 0.1, respectively, and variances such that the coefficient of variation is 0.5. Suppose new data is available to update this previous study via Bayes' Theorem. If maximizing the posterior PDF finds $\hat{\alpha} = 7.2$ and $\hat{\gamma} = 0.19$, then $\hat{y}(x) = 7.2x + 0.19$ is the most probable model in the linear model class.

The second level of analysis in Bayesian model class selection is finding the most probable model class among a set of proposed model classes (Beck and Yuen, 2004). Each model class has an associated evidence, which is the integral over the parameter space of the likelihood function weighted by the prior PDF (Equation 6.3). Thus

the evidence can be understood as the weighted average likelihood for the entire model class. It is also the normalizing constant in the definition of the posterior PDF (Equation 6.4; compare to Equation 6.1). Beck and Yuen (2004), Ching et al. (2005), and Muto (2006, Section 2.2) showed that the evidence can be decomposed into two terms that quantify how well the model class fits the data and the information gained from the data. The first term promotes models that predict the data well, whereas the second term promotes models with a simpler structure. The model class should provide a structure consistent with observations, but that structure should not be unnecessarily complex. Using Bayes' Theorem at the model class level, the probability of a model class can be quantified as the model class's evidence divided by the sum of the evidences for all proposed model classes (Equation 6.5), assuming all model classes are equally probable (Beck and Yuen, 2004). Bayesian model class selection compares multiple proposed model classes and selects the simplest model class (that is, extracts the least information from the data) that accounts for the available data.

$$EV_i = \int_B p(\beta_i \,|\, \mathcal{M}_i)\, p(\mathcal{D} \,|\, \beta_i, \mathcal{M}_i)\, d\beta_i \tag{6.3}$$

where $\mathcal{M}_i$ is the i$^{\text{th}}$ proposed model class,

EV_i is the evidence for $\mathcal{M}_i$,

and β_i is the most probable parameter values for $\mathcal{M}_i$.

$$\begin{aligned} \text{Posterior PDF} &= \frac{(\text{prior PDF})(\text{likelihood function})}{\text{evidence}} \\ p(\beta_i \,|\, \mathcal{D}, \mathcal{M}_i) &= \frac{p(\beta_i \,|\, \mathcal{M}_i)\, p(\mathcal{D} \,|\, \beta_i, \mathcal{M}_i)}{\int_B p(\beta_i \,|\, \mathcal{M}_i)\, p(\mathcal{D} \,|\, \beta_i, \mathcal{M}_i)\, d\beta}. \end{aligned} \tag{6.4}$$

$$p(\mathcal{M}_i \,|\, \mathcal{D}) = \frac{EV_i}{\sum_i EV_i}. \tag{6.5}$$

Returning to the previous example of the linear model class, now consider a second model class $y(x) = \delta x^2 + \zeta x + \eta$. Each of these two proposed model classes has an evidence based on prior information and the available data. If the data has a clear curvature in the x-y-plane, then the quadratic model class should be preferred. The evidence of the quadratic model class would be much larger than the evidence of the linear model because a quadratic model fits curved data much better than a linear model. However, if the output data is predominantly linear, the quadratic model class may fit the data slightly better, but the linear model class should be preferred because it extracts less information from the data (one fewer parameter). The evidence for each proposed model class quantifies this trade-off.

There are two practical considerations that apply to this procedure. For computational ease, I minimize the negative of the logarithm of the posterior PDF, which is an equivalent optimization to maximizing the posterior PDF. Also, I apply a Laplace approximation to evaluate the evidence (Equation 6.6). The Laplace approximation idealizes the posterior PDF as a multidimensional Gaussian, which has an integral with a closed form (Beck and Yuen, 2004). Thus, this approximation is best for surfaces with a single peak; the model class is said to be globally identifiable.

$$\begin{aligned} EV &= \int_B p(\beta \,|\, \mathcal{M})\, p(\mathcal{D} \,|\, \beta, \mathcal{M})\, d\beta \\ &\approx (2\pi)^{(N_B+1)/2} p(\mathcal{D} \,|\, \hat{\beta}, \mathcal{M}) \left|\hat{H}\right|^{-1/2} \end{aligned} \tag{6.6}$$

where $\hat{H}$ is the Hessian of the negative of the logarithm of the product of the prior PDF and the likelihood function, evaluated at $\hat{\beta}$.

6.2.3 Application

I apply Bayesian model class selection to two sets of proposed building response models. I select one model to predict collapse given a value of intensity measure; I select a second model to predict whether the building is a total structural loss (including collapse) in a ground motion with a given intensity measurement; and I select a third

model to predict the peak IDR, assuming the building is not a total structural loss in a ground motion with a given intensity measurement. The intensity measure may be a vector quantity. I distinguish between these three building response measures (that is, collapse, total structural loss, and peak IDR) because they categorize or quantify three distinct building responses.

The data suggest forms for the prediction models. Figures 6.9–6.11 plot the building responses as functions of three intensity measures: pseudo-spectral acceleration (PSA), peak ground displacement, and peak ground velocity. PSA may predict building response well because it is commonly used to characterize seismic hazard and building response. Peak ground measures, however, are independent of a particular building and are more broadband measures of strong ground motions. The data suggest that collapse and total structural loss can be modeled with a sigmoidal function of the intensity measures. The peak IDR seems to be a linear function of the considered intensity measures with a log-normal distribution about the expected peak IDR. Figure 6.12 shows the distribution of peak IDR about a line through the data as functions of $\mathrm{PGD}_{\mathrm{lp}}$ and $\mathrm{PGV}_{\mathrm{lp}}$. These distributions appear log-normal in shape.

Equations 6.7 define the four proposed model classes to predict collapse and total structural loss from the ground motion intensity measures. These equations have the functional form of a sigmoid, which is approximately zero for small values of intensity measures and approximately one for large values. The four models consider polynomials of the three intensity measures as well as polynomials of their logarithms. Equations 6.8 define the four model classes to predict peak IDR from the intensity measures. The form of the argument of the exponentials in Equation 6.7 is similar to the form of the models to predict peak IDR.

$$
\begin{aligned}
\mathcal{M}_1\text{: } p(\text{state}) &= \left[1 + \exp\left(-\alpha_0 - \alpha_1 \ln PSA\right)\right]^{-1} \\
\mathcal{M}_2\text{: } p(\text{state}) &= \left[1 + \exp\left(-\alpha_0 - \alpha_1 PGD_{\mathrm{lp}} - \alpha_2 PGV_{\mathrm{lp}} - \alpha_3 PGD_{\mathrm{lp}} PGV_{\mathrm{lp}}\right)\right]^{-1} \\
\mathcal{M}_3\text{: } p(\text{state}) &= \left[1 + \exp\left(-\alpha_0 - \alpha_1 \ln PGD_{\mathrm{lp}} - \alpha_2 \ln PGV_{\mathrm{lp}} - \alpha_3 \ln PGD_{\mathrm{lp}} \ln PGV_{\mathrm{lp}}\right)\right]^{-1}
\end{aligned}
$$

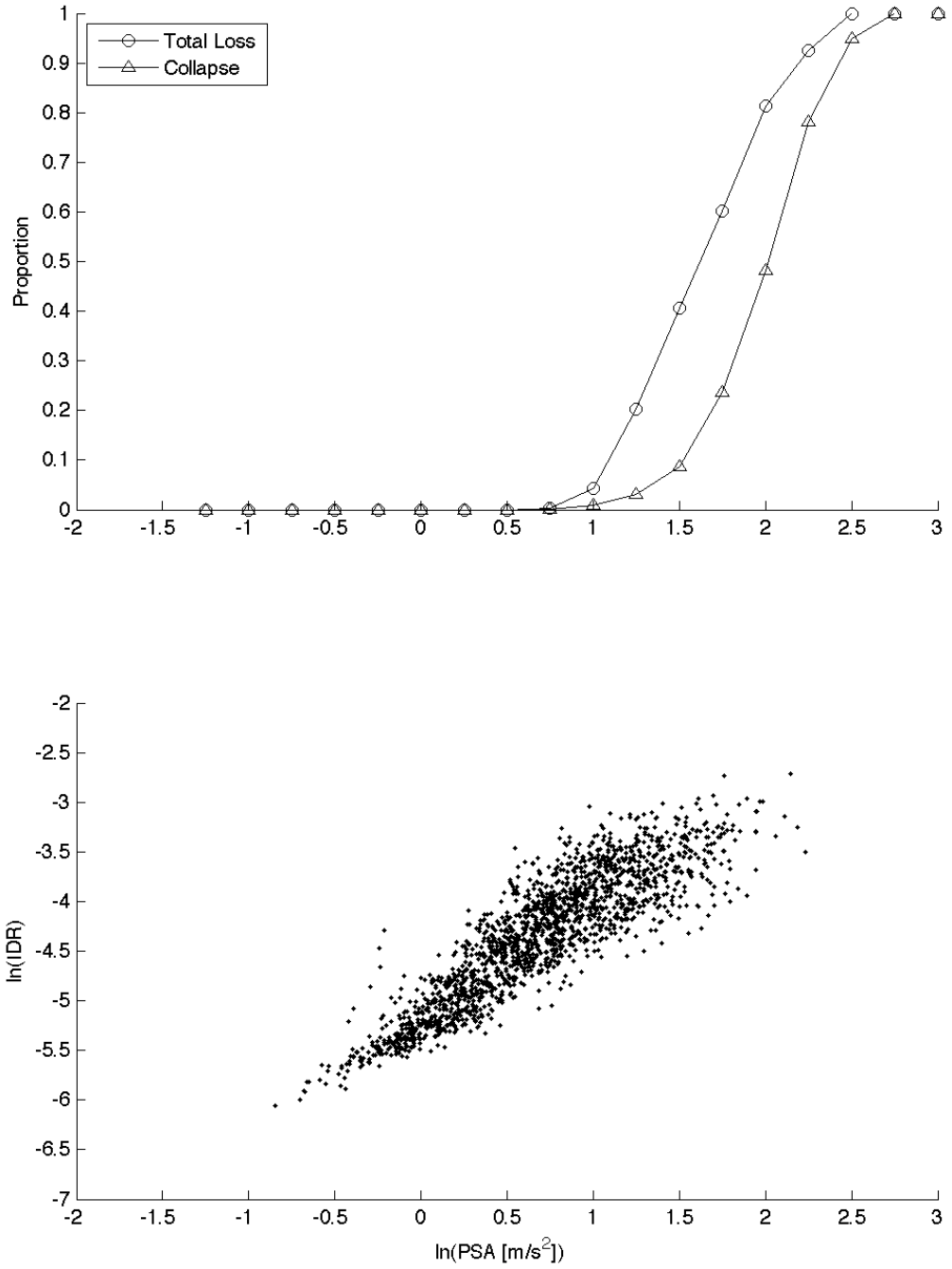

Figure 6.9: The simulation data suggest that PSA may predict building response well. The proportions of total structural loss and collapse appear to smoothly vary from zero to one as a function of log-PSA. The log-peak IDR varies linearly with log-PSA, but the variance about that line generally increases with log-PSA.

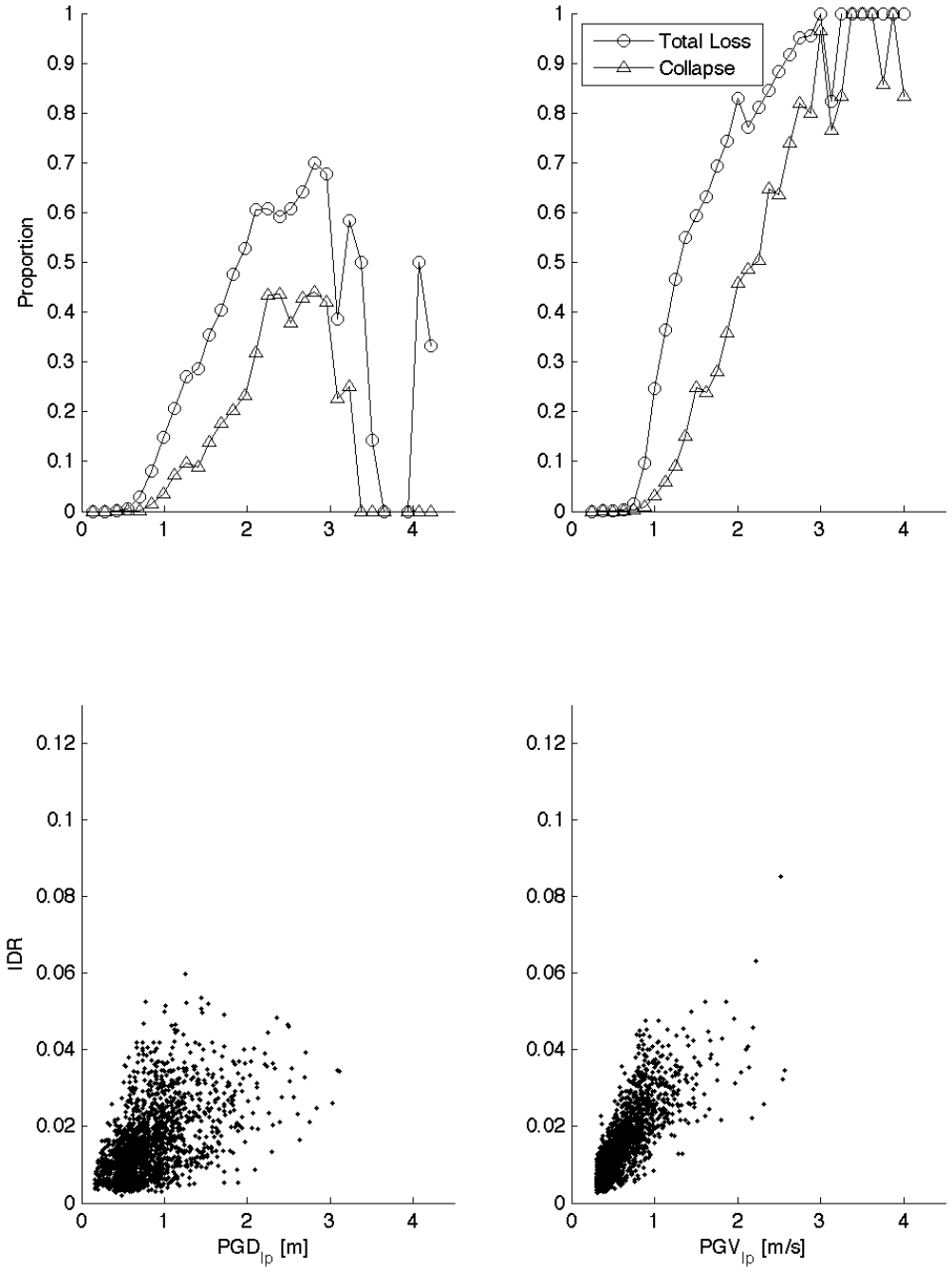

Figure 6.10: This figure projects some of the building response data onto the PGD_{lp}-response and PGV_{lp}-response planes. The proportions of total structural loss and collapse do not vary smoothly for PGD_{lp} greater than 3 m and PGV_{lp} greater than 3 m/s. The data are sparse for such strong ground motions. Peak IDR apparently increases linearly with PGD and PGV, but the variances are large.

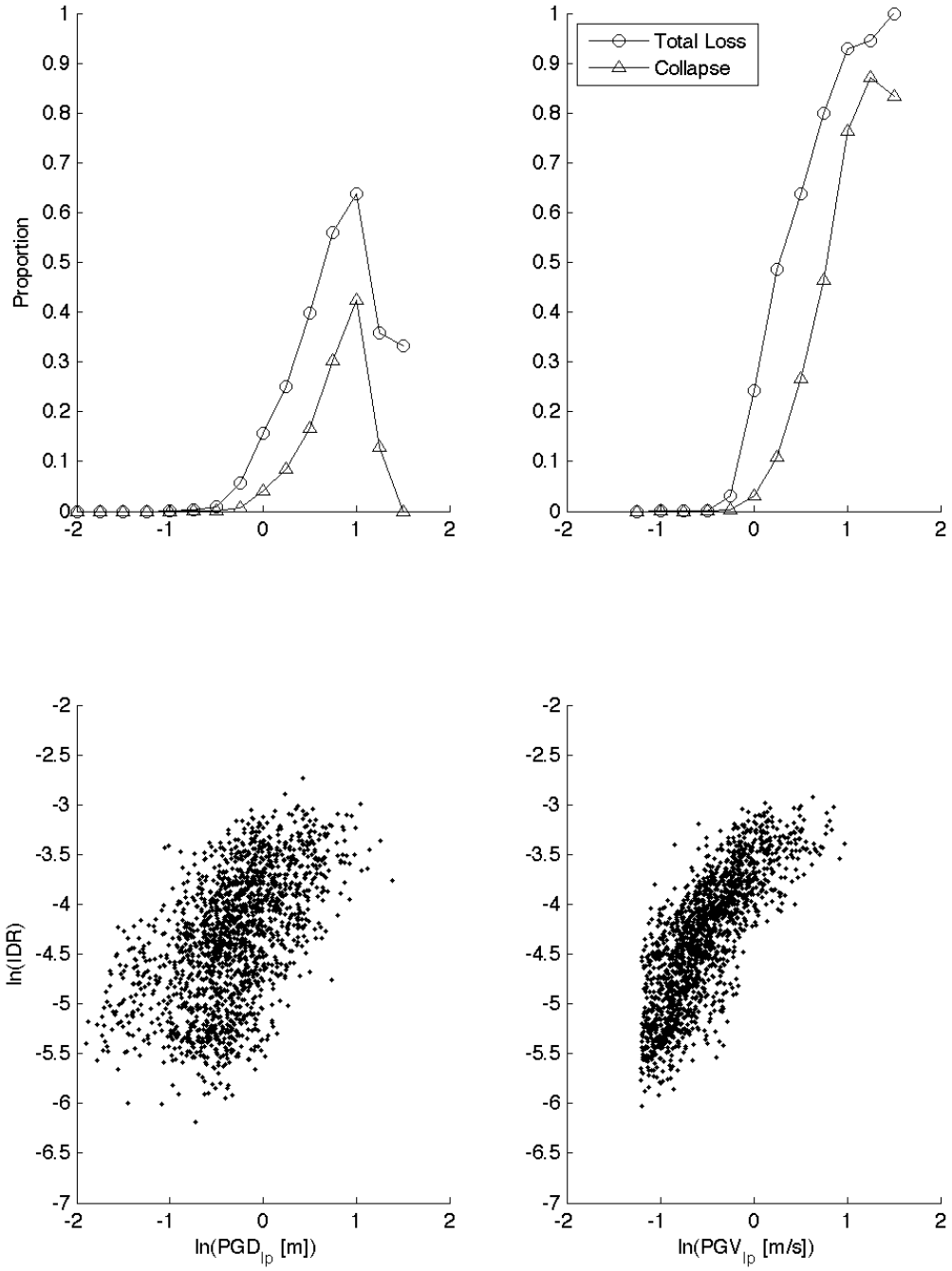

Figure 6.11: This figure shows the building responses as functions of log-PGD_{lp} and log-PGV_{lp}. The proportions of total structural loss and collapse generally increase with log-PGD_{lp} and log-PGV_{lp}. The log-peak IDR varies linearly as a function of log-PGD_{lp} and log-PGV_{lp} with approximately constant variances.

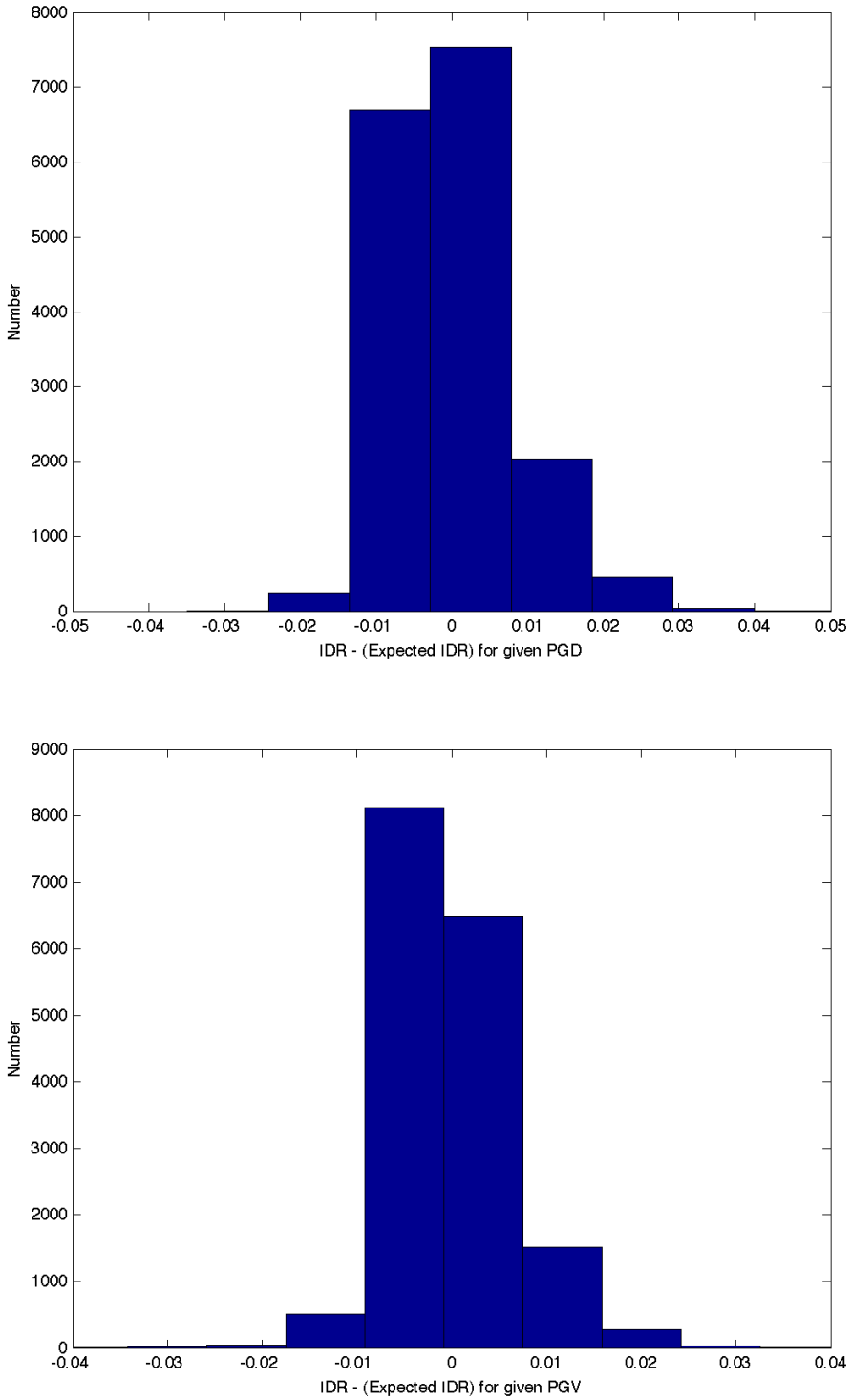

Figure 6.12: The peak IDR prediction models in this thesis predict the median peak IDR as well as a measure of the uncertainty. The data suggest that the distribution of peak IDR about a line through the data (that is, the expected peak IDR) is log-normal for given values of peak ground displacement and velocity.

$$\begin{aligned} \mathcal{M}_4\text{: } p(\text{state}) &= [1 + \exp(-\alpha_0 - \alpha_1 \ln PGV_{\text{lp}})]^{-1} \\ &\quad \text{where state is either collapse or total structural loss} \\ &\quad \text{given a value of intensity measure.} \end{aligned} \tag{6.7}$$

$$\begin{aligned} \mathcal{M}_1\text{: } \ln PeakIDR &= \beta_0 + \beta_1 \ln PSA + \epsilon_1 \\ \mathcal{M}_2\text{: } \ln PeakIDR &= \ln(\beta_1 PGD_{\text{lp}} + \beta_2 PGV_{\text{lp}} + \beta_3 PGD_{\text{lp}} PGV_{\text{lp}}) + \epsilon_2 \\ \mathcal{M}_3\text{: } \ln PeakIDR &= \beta_0 + \beta_1 \ln PGD_{\text{lp}} + \beta_2 \ln PGV_{\text{lp}} + \beta_3 \ln PGD_{\text{lp}} \ln PGV_{\text{lp}} + \epsilon_3 \\ \mathcal{M}_4\text{: } \ln PeakIDR &= \beta_0 + \beta_1 \ln PGV_{\text{lp}} + \epsilon_4 \\ &\quad \text{where the peak IDR assumes the building is repairable} \\ &\quad \text{and } \epsilon_i \sim \mathcal{N}(0, \sigma_i^2). \end{aligned} \tag{6.8}$$

Prior information about the parameter values completes the specification of each model class for Bayesian model class selection. I assume the parameters are independent, and each is normally distributed. I choose a value for the prior mean of each parameter based on the character of the data in Figures 6.9–6.11. I choose a fairly wide, Gaussian distribution about the mean, defined as a coefficient of variation equal to one-third. This definition of prior information does not significantly affect the Bayesian model class selection in this application. The amount of data used in the model class selection contributes significantly more evidence to the model than does the prior definition.

For each of the four building designs with fracture-prone or sound welds, I maximize the posterior PDF for each proposed model in Equations 6.7 and 6.8. Figures 6.13–6.17 show the proposed models with the most likely parameter values plotted with the data. Figures 6.13 and 6.14 show the models based on PSA for collapse, total structural loss, and peak IDR. Note that these figures show the complete models as functions of PSA (unlike the next figures which show contours of the prediction models). Figures 6.15–6.17 present the three models based on PGD_{lp} and PGV_{lp}

for collapse, total structural loss, and peak IDR, respectively. Models 2 and 3 are functions of both PGD_{lp} and PGV_{lp}, making the predicted building response a three-dimensional surface. Model 4 is a function of PGV_{lp} alone. To compare the prediction models, I show the contour where the probability of collapse or total structural loss is 0.3.

Figures 6.15 and 6.16 show that the separating contours (here defined as a 30% probability of collapse or total structural loss) for Models 2–4 are similar where there is available data. Consider the separating contours for the responses of the six-story buildings. Where there is no available data, the separating contours diverge. Model 2 curves toward the origin; the separating contour intersects the abscissa and ordinate. Model 3 curves away from the origin; the separating contour appears to approach the PGD and PGV axes for values of PGD and PGV greater than those considered here. Model 4 is only a function of PGV. For the twenty-story models, the separating contours for Models 2–4 appear similar and almost independent of PGD, suggesting that PGD is not needed in the building response prediction models.

Table 6.1 reports the probabilities for the collapse prediction models. For all building models, collapse prediction Model 1 is the least likely structure for the data. For two building models (J6B and J6P) Model 2 is the most likely collapse prediction model. For two other building models (U6P and U20B) Model 3 is the most likely collapse prediction model. For the remaining four building models (J20B, J20P, U6B, and U20P) Model 4 is the most likely collapse prediction model. No proposed model is consistently most likely to predict collapse.

Table 6.2 reports the probabilities for the total structural loss prediction models. Again, no proposed prediction model is consistently the most likely to predict total structural loss. Model 1 is most likely to predict total structural loss for three buildings: J6P, J20P, and U6P. Model 2 is never the most likely to predict total structural loss. Model 3 is most likely to predict total structural loss in two buildings: U20B and U20P. Model 4 is most likely for three buildings: J6B, J20B, and U6B. The Bayesian model class selection criterion does not consistently select the same functional form for all four building designs and for both weld states.

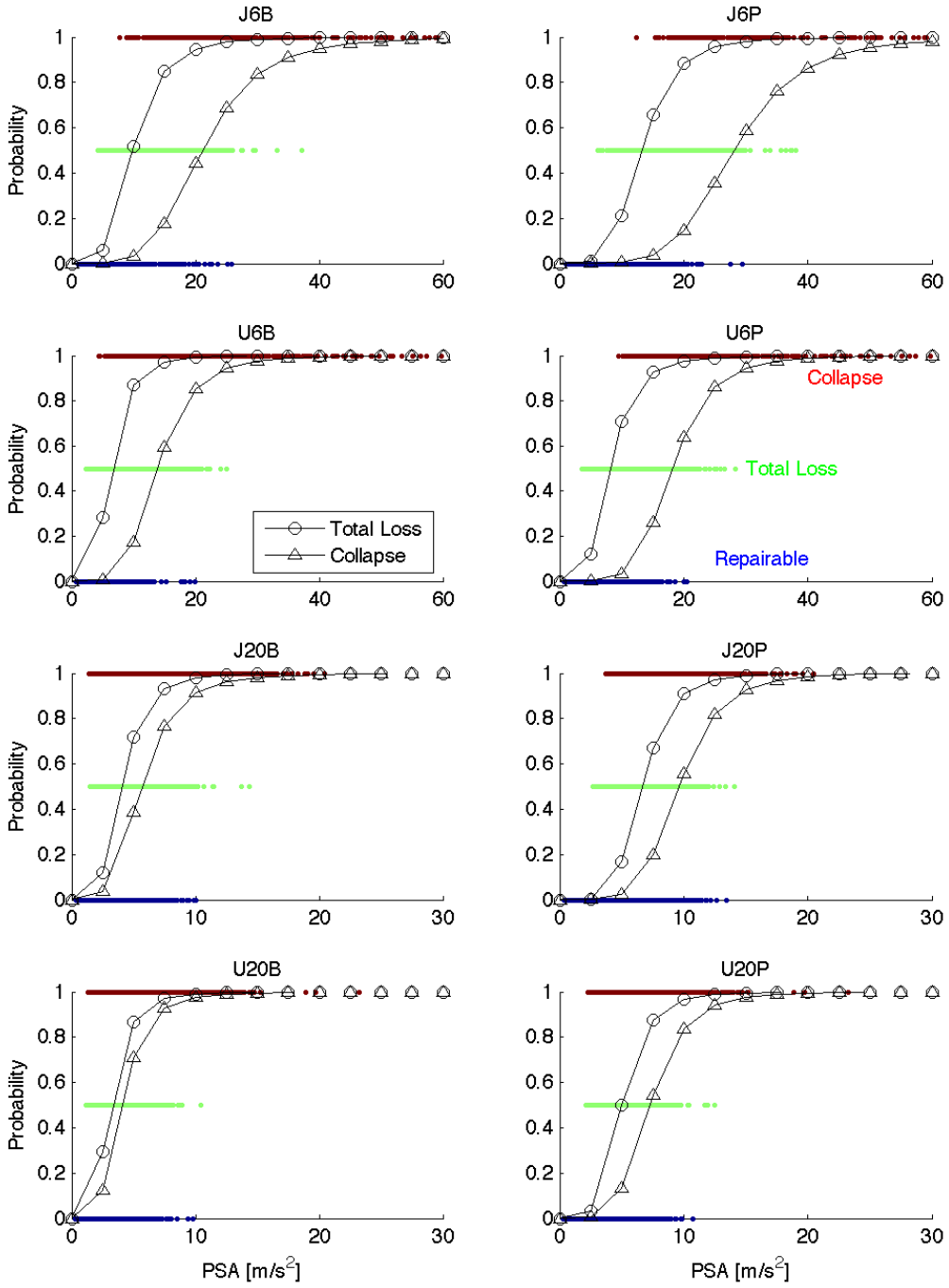

Figure 6.13: This figure locates the collapse, total structural loss, and repairable building response data as functions of PSA. I locate the data at probabilities of 1, 0.5, and 0, respectively, to distinguish what PSAs result in each response and to suggest how well the collapse and total structural loss models distinguish the building states. The black lines with symbols show Model 1 with the most probable parameter values for collapse and total structural loss. For the twenty-story buildings with brittle welds (J20B and U20B), the total structural loss and collapse models are almost the same.

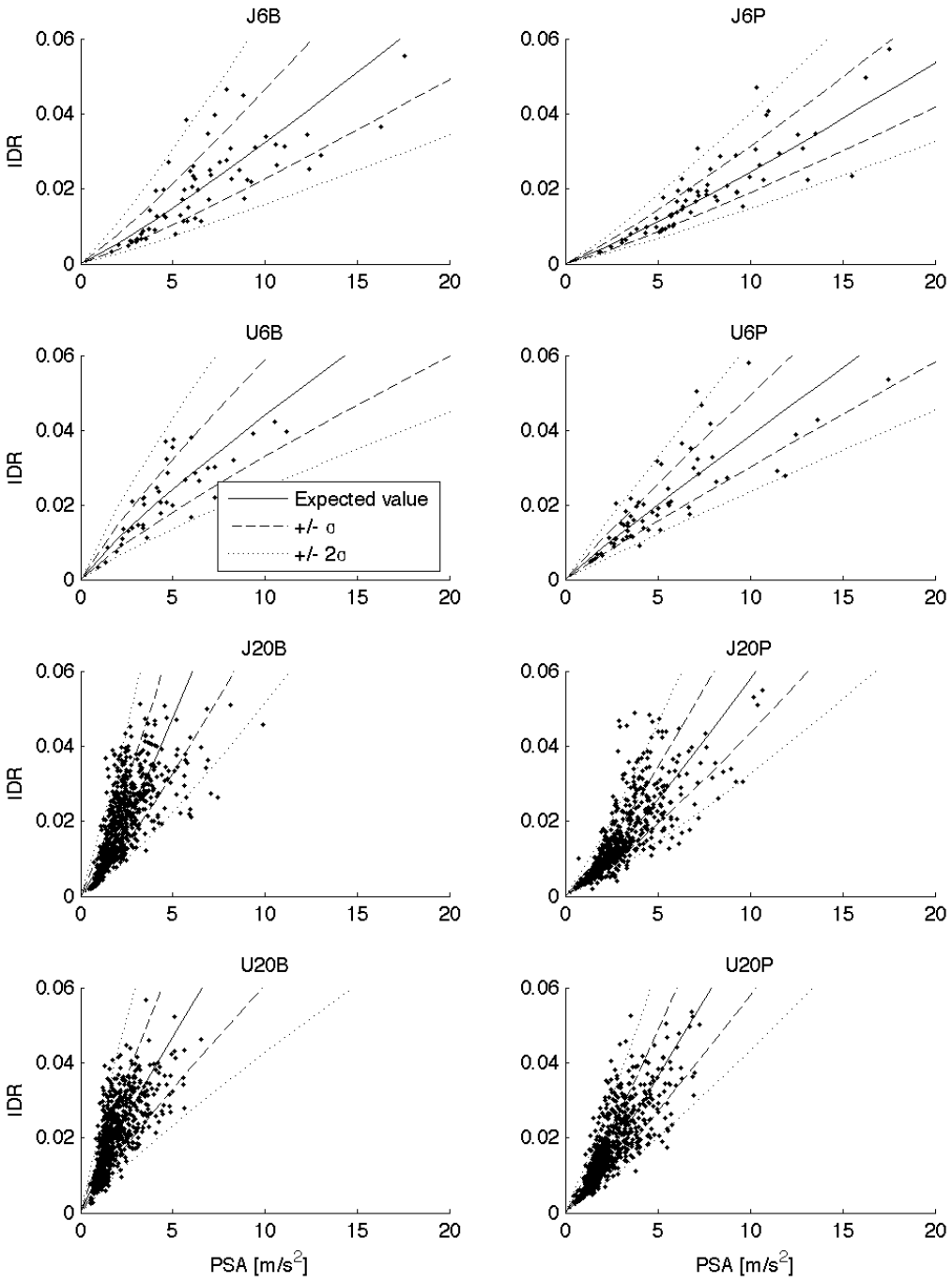

Figure 6.14: This figure shows the peak IDR data as a function of PSA. The lines indicate the prediction models with the most likely parameter values from the maximum posterior PDF analysis.

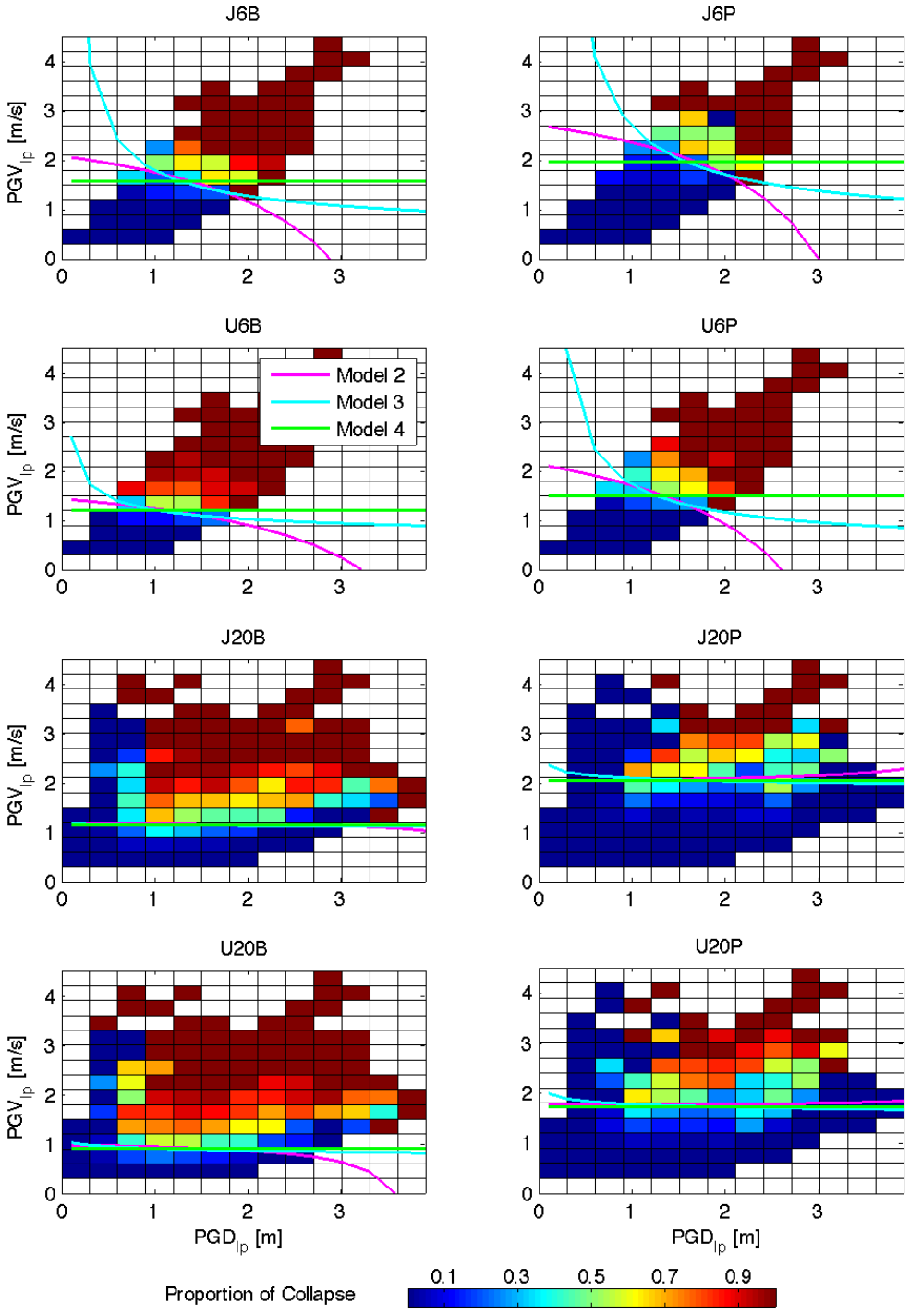

Figure 6.15: This figure compares the collapse prediction models with the most likely parameter values to the data. The contours represent a predicted collapse probability of 0.3 for Models 2–4. Note how similar the predictions of these models are where there is available data.

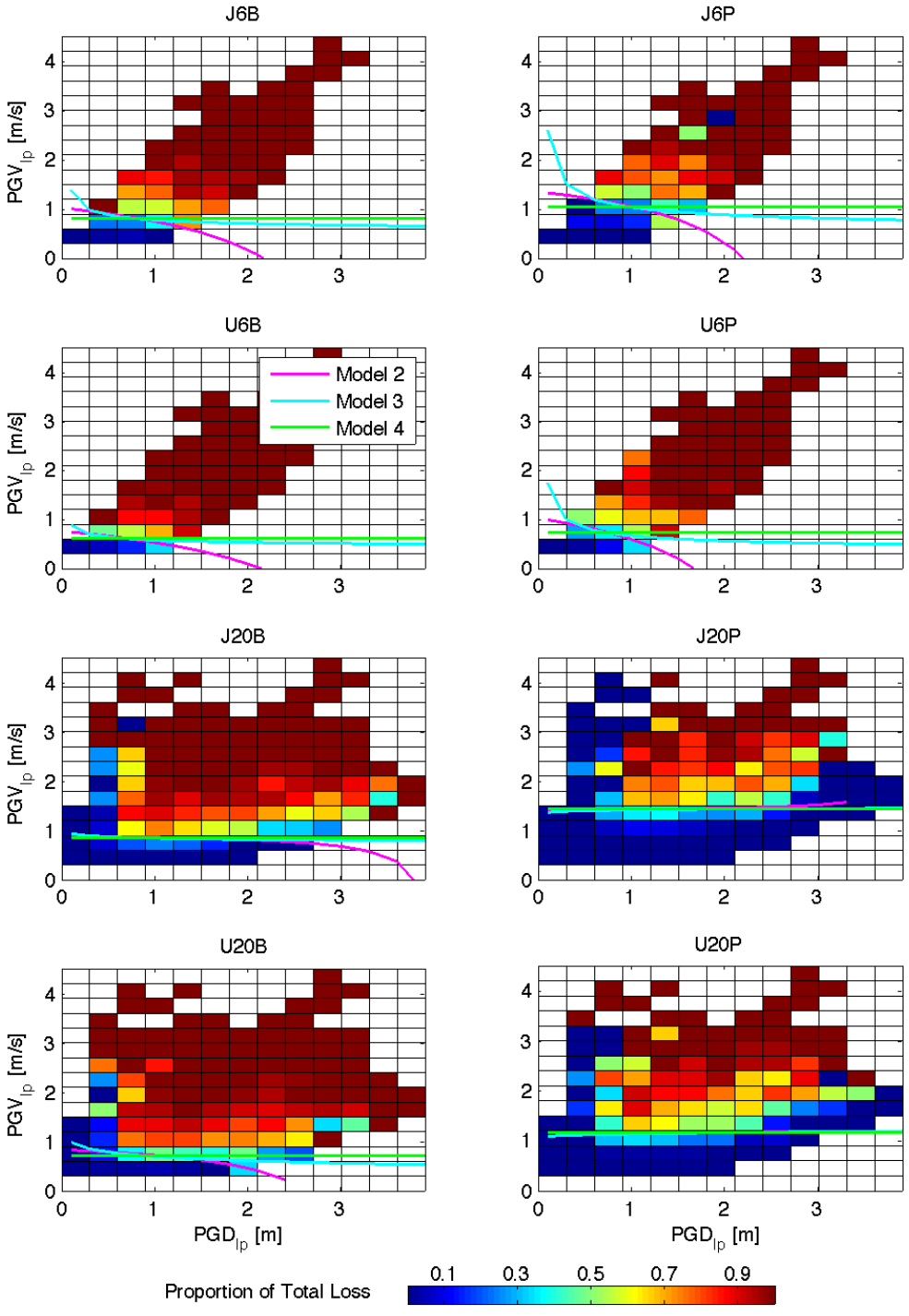

Figure 6.16: This figure compares the total structural loss prediction models with the most likely parameter values to the data. The contours represent a probability of total structural loss of 0.3 for Models 2–4.

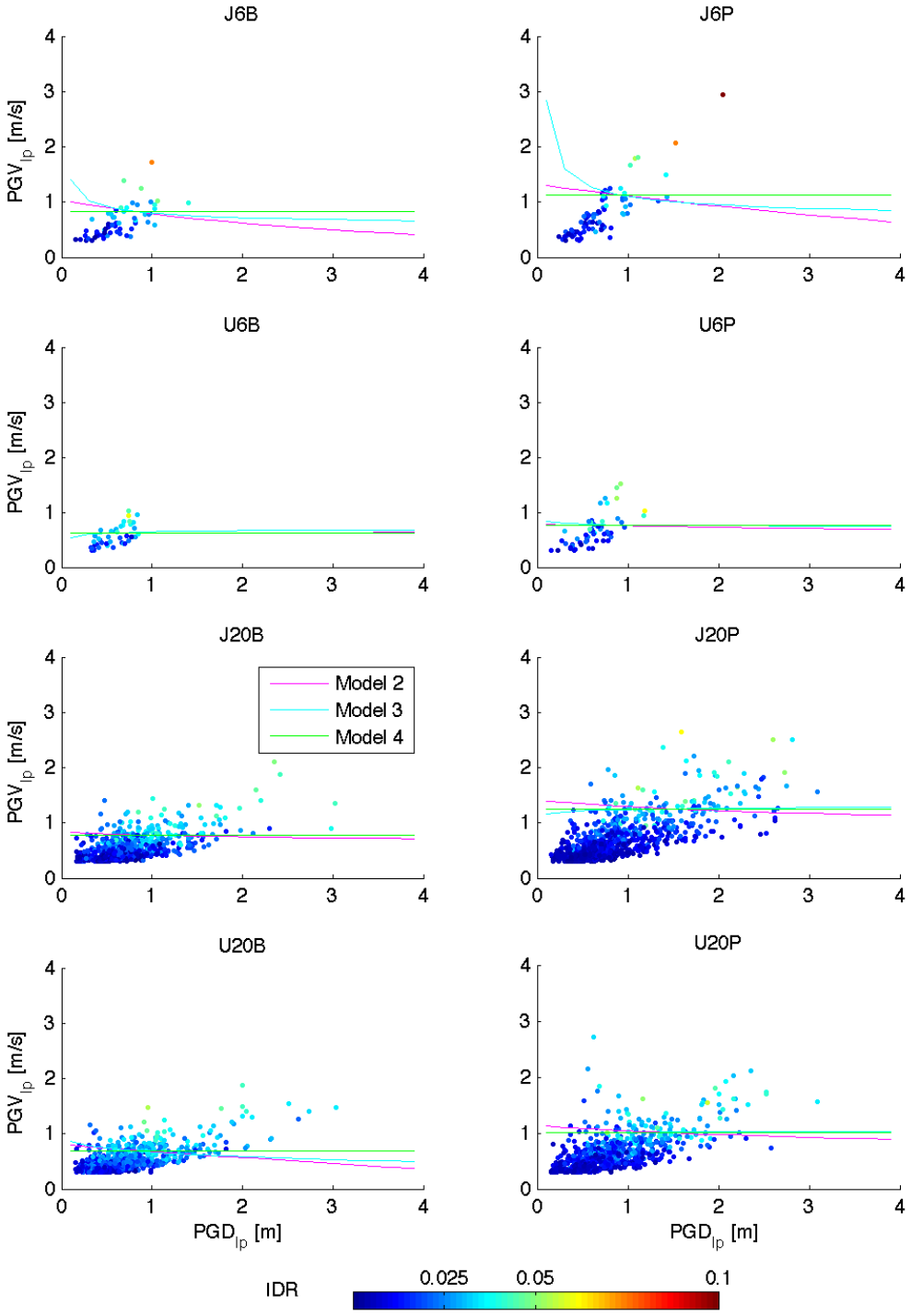

Figure 6.17: This figure compares the peak IDR prediction models with the most likely parameter values to the data. The contours represent a predicted peak IDR of 0.025, the FEMA 356 level for life safety. Again, note the similar predictions where there is available data.

Model	*J6B*	*J6P*	*J20B*	*J20P*
1	0.0	0.0	0.0	0.033
2	**0.92**	**1.0**	0.0	0.0
3	0.077	0.0	0.0	0.0
4	0.0	0.0	**1.0**	**0.97**
Model	*U6B*	*U6P*	*U20B*	*U20P*
1	0.0	0.0	0.0	0.0
2	0.013	0.0027	0.0	0.0
3	0.14	**1.0**	**0.95**	0.0
4	**0.84**	0.0	0.048	**1.0**

Table 6.1: This table reports the probabilities of each proposed collapse prediction model. None of the four proposed models is consistently most likely for all building designs and weld states.

Model	*J6B*	*J6P*	*J20B*	*J20P*
1	0.0	**1.0**	0.0	**1.0**
2	0.0	0.0	0.0	0.0
3	0.25	0.0	0.00051	0.0
4	**0.75**	0.0	**1.0**	0.0
Model	*U6B*	*U6P*	*U20B*	*U20P*
1	0.0	**1.0**	0.0	0.0
2	0.040	0.0	0.0	0.0
3	0.00017	0.0	**1.0**	**1.0**
4	**0.96**	0.0	0.0	0.0

Table 6.2: This table reports the probabilities of the proposed total structural loss models. As with the collapse prediction models, no proposed total structural loss model is consistently best for all building models.

Model	*J6B*	*J6P*	*J20B*	*J20P*
1	1.0	1.0	1.0	1.0
2	0.0	0.0	0.0	0.0
3	0.0	0.0	0.0	0.0
4	0.0	0.0	0.0	0.0
Model	*U6B*	*U6P*	*U20B*	*U20P*
1	1.0	1.0	1.0	1.0
2	0.0	0.0	0.0	0.0
3	0.0	0.0	0.0	0.0
4	0.0	0.0	0.0	0.0

Table 6.3: This table reports the probabilities of the proposed peak inter-story drift ratio prediction models. The prediction model based on pseudo-spectral acceleration is the most likely building response prediction model for all considered buildings.

Table 6.3 reports the model probabilities for the prediction of peak IDR given that the building is not a total structural loss. For all building models, the model based on PSA is most likely to predict peak IDR. This result should not be surprising because PSA filters the ground motion at the fundamental period of each building. Thus PSA is a good characterization of ground motion for mildly to moderately inelastic building responses.

6.2.4 Interpretation

The building response prediction models for a categorical state (that is, collapse or standing and total structural loss or repairable) define a probability that the building assumes a particular state. Ideally a separating curve could be drawn at a value of intensity measure to properly categorize the building states, keeping in mind that the intensity measure could be a vector quantity. For intensity measures below the curve, the buildings do not collapse or are not a total structural loss, and for intensity measures above the curve, the buildings collapse or are a total structural loss. The models in this thesis quantify the probability of the state, rather than drawing a distinct demarcation between the states. Considering the data, a curve is not justified: for a relatively large range of intensity measures, both states are possible simultaneously. Drawing a single line to separate the states would result in a large number of

misclassifications. A better characterization of the states is to provide a probability of the state for a given value of intensity measure.

The most successful categorical model will have the steepest slope separating the states. The ideal model has an infinite slope, corresponding to the clear demarcation between the states. As the slope decreases, the distinction between the states becomes less clear. In the extreme, a large change in the intensity measure causes a small change in the probability of the state. The data in this thesis do not support this characterization: by visual inspection of Figures 6.6, 6.7, and 6.13, there is a narrow band of intensity measure values on which different simulations predict both states. That is, for the same value of intensity measure, the building may collapse or stand or may be a total structural loss or repairable. The Bayesian model class selection procedure implicitly accounts for this consideration, since a model with a slope that is too small will not accurately predict the building state.

Even though a probabilistic statement about the categorical state of a building is more informative, there are times when a line must be drawn, figuratively and literally. The choice of the curve that separates the two states of building response reflects a value judgement. One person may be willing to accept a probability of 0.5 that the building will collapse. A second person may be more cautious and judge a probability of 0.1 as sufficiently risky. For this thesis, I consider a probability of 0.3 to be the separating curve, or separating contour, between collapse and standing and between total structural loss and repairable. I use this separating contour to compare the predictions of the proposed models and to compare the performance of the building models. The choice of a specific probability would not significantly affect the location of the separating contour for models with a steep slope, but it would affect that location for models with shallow slopes.

The most direct way to use the building response prediction models in this thesis is to employ the most likely model according to the metric of Bayesian model class selection. The selection procedure quantifies the probability of each proposed model, and for the proposed models in this thesis, one prediction model is obviously most likely for each building model. To predict the response of a building similar to one of

Collapse Model 3 Parameter Estimates				
Building	α_0	α_1	α_2	α_3
J6B	-4.1	2.6	5.7	0.88
J6P	-5.3	2.4	4.5	0.96
U6B	-2.2	1.6	7.0	0.80
U6P	-3.7	2.8	5.3	0.90
J20B	-1.5	0.092	4.9	-0.076
J20P	-5.0	-0.12	5.6	0.48
U20B	-0.41	0.24	4.4	-0.45
U20P	-3.6	0.11	4.7	0.18

Table 6.4: This table provides the most likely values for the parameters in collapse prediction Model 3.

Total Structural Loss Model 3 Parameter Estimates				
Building	α_0	α_1	α_2	α_3
J6B	0.26	0.86	4.4	0.76
J6P	-0.99	1.0	4.1	0.66
U6B	2.0	1.0	5.2	0.65
U6P	0.72	1.3	3.9	0.61
J20B	0.088	0.23	5.5	-0.16
J20P	-2.9	0.0021	5.8	-0.29
U20B	0.83	0.69	4.7	-0.42
U20P	-1.6	-0.013	5.3	-0.98

Table 6.5: This table lists the most likely values for the parameters in Model 3 to predict whether a building is a total structural loss.

those considered, consult Tables 6.1–6.3 to find the most likely proposed model, and then find the values of the parameters from the tables in Appendix B. This approach ensures that the employed prediction model is more probable than the other four proposed models for the building under consideration.

A single functional form for steel moment frame response prediction is simpler and more intuitive than choosing the most likely model according to a metric. The Bayesian model class selection criterion should inform the decision of which functional form to choose to predict the building response, but there are other considerations as well. The prediction model should be consistent with a physical understanding of the underlying problem. The recommended model may be extrapolated beyond the currently available data, and thus a model consistent with the underlying physical

Peak IDR Model 1 Parameter Values			
Building	β_0	β_1	σ^2
J6B	-6.0	1.1	0.13
J6P	-6.3	1.1	0.062
U6B	-5.1	0.86	0.084
U6P	-5.4	0.95	0.061
J20B	-5.0	1.2	0.14
J20P	-5.5	1.2	0.083
U20B	-4.5	0.87	0.12
U20P	-5.1	1.1	0.087

Table 6.6: This table presents the most likely values of the parameters for the most likely prediction model for peak inter-story drift ratio.

behavior should be preferred. (This is not, however, an endorsement of extrapolation.) The preferred model class should also have a low rate of misclassification.

Model 1 provides some physical insight into the patterns of building response as a function of pseudo-spectral acceleration. Figure 6.13 compares the predictions of Model 1 for total structural loss and collapse. Note the relative locations of the total structural loss and collapse curves for the eight building models. For the six-story buildings, the two curves are relatively far apart: the pseudo-spectral acceleration must increase by 10–15 m/s^2 for a building with perfect welds to go from total structural loss to collapse or increase by 5–10 m/s^2 for a building with brittle welds. The increase in pseudo-spectral acceleration required for a building to go from a total structural loss to collapse is smaller for the twenty-story buildings. For buildings with brittle welds, this increase in pseudo-spectral acceleration is smaller than for buildings with perfect welds. Twenty-story buildings with brittle welds need only a small change in pseudo-spectral acceleration for a total structural loss to become a collapse. Similar statements about the relative performance of the buildings can be made for the peak ground measures, too.

Model 1 is consistently less likely to accurately predict collapse or total structural loss than Models 2–4. Pseudo-spectral acceleration filters the ground motion at the fundamental period of the building. For small ground motions, the building remains elastic, and a spectral characterization of the ground motion accurately predicts build-

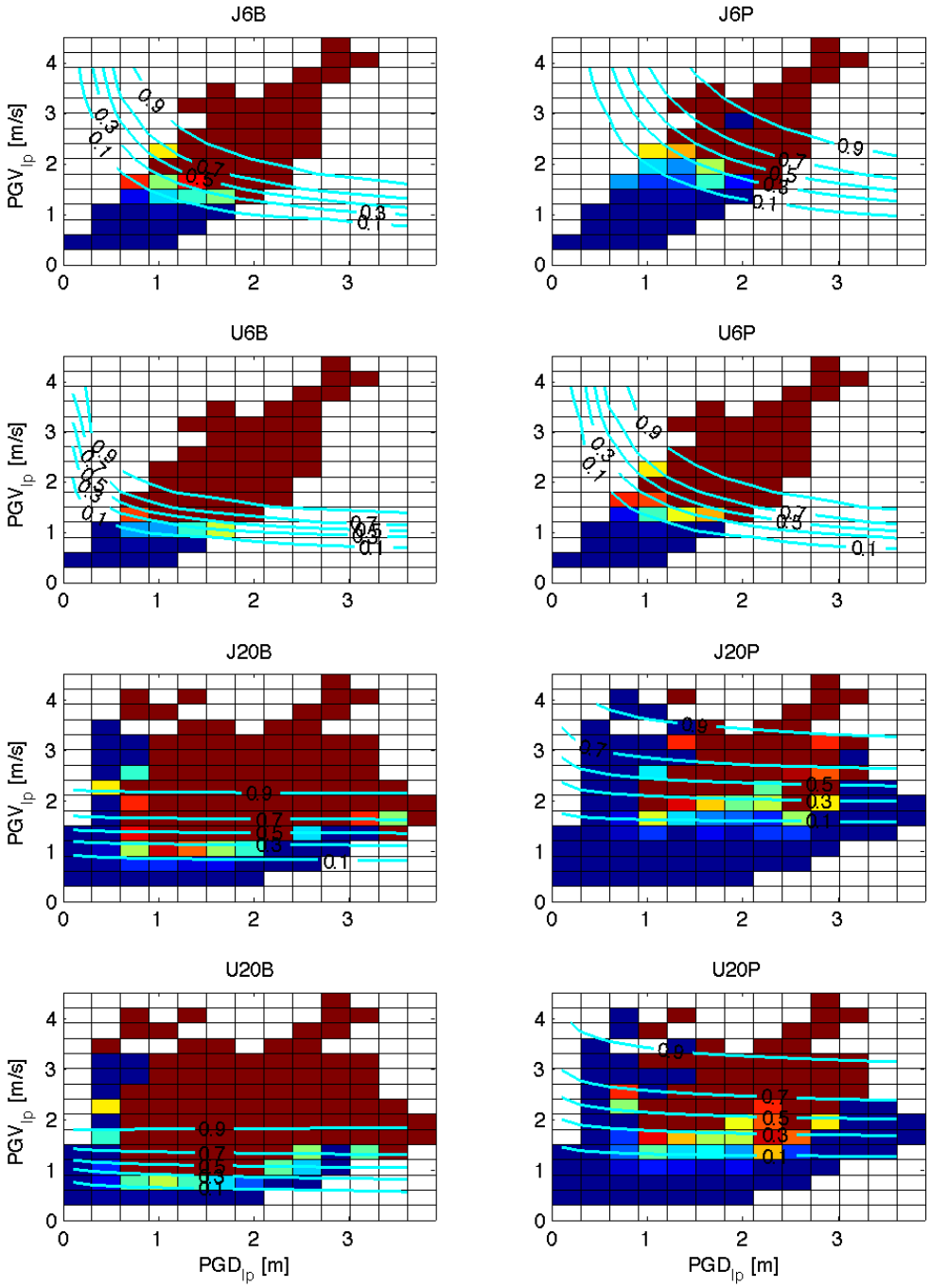

Figure 6.18: This figure compares the contours of Model 3 at 10, 30, 50, 70, and 90% probabilities of collapse to the data. For the six-story buildings (top four subfigures), the contours are close, indicating that the model classifies collapse or standing well. For the twenty-story buildings (bottom four subfigures), the contours are more widely spaced. Also, these contours do not distinguish the twenty-story buildings that do not collapse in peak ground displacements less than 0.6 m.

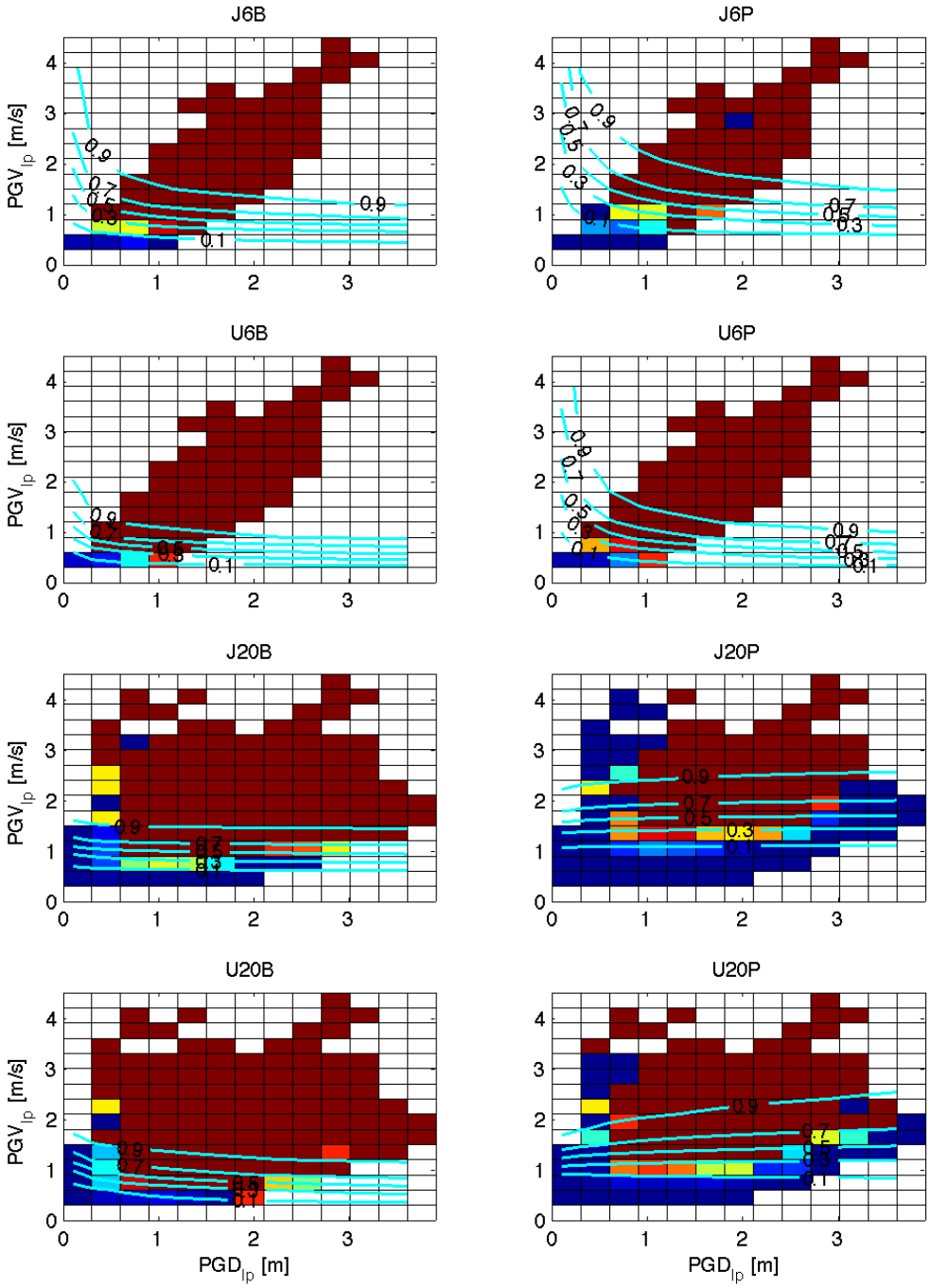

Figure 6.19: Similar to Figure 6.18, this figure compares the contours of Model 3 at 10, 30, 50, 70, and 90% probabilities of total structural loss to the data. This model seems to characterize the data well, even though Bayesian model class selection does not consistently rank it most probable. For some building models, the building response prediction models based on pseudo-spectral acceleration or peak ground velocity alone are more probable than this model, which is a function of both peak ground displacement and velocity.

ing response. In strong ground motions, the building exceeds its yield strength and accumulates damage. The fundamental period of a building accumulating damage lengthens as the building softens. The characterization of the ground motion at the elastic fundamental period does not accurately predict inelastic building response. For severely inelastic building responses, such as total structural loss and collapse, an intensity measure based on a filter with a narrow band of periods does not predict building response as well as a more broadband measure such as the peak ground motion measures.

Models 2–4 tend to be the most likely prediction models for collapse and total structural loss. Section 6.2.3 discusses the curvature of these models in the PGD-PGV plane. Physically, Model 3 better describes steel moment frame response in strong ground motions because it curves away from the origin. Ground motions with a large PGD and a small PGV imply that the ground is slowly moving a large distance. In this type of ground motion, the building would follow the ground motion as an approximately rigid body with only small deformations. High frequencies tend to dominate ground motions with a small PGD and a large PGV. Tall steel moment frames are not significantly affected by short-period ground motions, so the building responses in this type of ground motion would be small. Model 3 describes these physical building responses because it allows low probabilities of collapse or total structural loss for both types of ground motions, unlike Models 2 and 4. This consideration is more important for the six-story building response prediction models since there is less available data to constrain the model, compared to the data for the twenty-story models.

The misclassification of the available data using the prediction models also indicates the predictive power of the categorical models. I use the separating contour where the collapse probability is 0.3 to categorize the available data as collapsed or standing and as total structural loss or repairable. Tables 6.7 and 6.8 list the percentage of the data misclassified by the four models. The model using pseudo-spectral acceleration to predict building response (Model 1) has a higher rate of misclassification compared to the other four models. Among Models 2–4 there are similar rates

Misclassification of Collapse Data [% of Available Data]				
Building	*Model 1*	*Model 2*	*Model 3*	*Model 4*
J6B	9.4	6.3	6.5	7.4
J6P	4.6	3.7	3.9	4.4
U6B	13	8.1	8.3	8.5
U6P	8.8	7.0	7.5	7.8
J20B	10.	9.2	9.5	9.5
J20P	2.9	2.7	2.8	2.9
U20B	14	13	13	13
U20P	4.8	4.7	4.9	4.9

Table 6.7: I use the proposed prediction models to classify the available data as collapsed or standing. Model 1 misclassifies collapse data more often than Models 2–4.

Misclassification of Total Structural Loss Data [% of Available Data]				
Building	*Model 1*	*Model 2*	*Model 3*	*Model 4*
J6B	18	18	19	19
J6P	14	16	16	17
U6B	16	15	15	15
U6P	17	19	19	19
J20B	15	11	11	11
J20P	6.0	5.8	6.0	6.0
U20B	19	15	15	15
U20P	9.9	8.8	8.9	8.8

Table 6.8: Similar to Table 6.7, I use the proposed models to categorize the available data as total structural loss or repairable. The rate of misclassification is much larger for the total structural loss models than for the collapse models.

of misclassification.

Of the four proposed building response prediction models of the categorical states, I prefer Model 3. Bayesian model class selection recommends it for several building types. The functional form of the model is consistent with a physical understanding of the response of tall steel moment frames in strong ground motions, and there is a low rate of misclassification. However, depending on the specific application, Model 2 or 4 may be useful to predict collapse or total structural loss responses.

Model 1 should be preferred to predict the peak inter-story drift ratio, assuming that the building is not a total structural loss in a given ground motion. The probability of this model is consistently 1 using the Bayesian model class selection criterion.

Pseudo-spectral acceleration is also widely used in the earthquake engineering community to characterize seismic risk and building response. The interpretation of building response as a function of spectral quantities has a sound physical explanation.

The building response prediction models developed in this chapter predict the same relative building performance as seen in the data. Figure 6.20 compares the collapse separating contours for the four building designs with perfect or brittle welds. The stiffer, higher-strength designs have separating contours that vary with both PGD and PGV. The more flexible, lower-strength designs, however, are almost independent of PGD. According to these prediction models, a ground motion with large PGV but small PGD would collapse the more flexible, and not the stiffer, design. A ground motion with large PGD but small PGV tends to collapse the buildings with stiffer designs and not those with more flexible designs. The six-story buildings require larger ground motions than the twenty-story buildings to collapse. The presence of brittle welds shifts the separating contours to smaller combinations of peak ground motion responses. The effect of brittle welds on the stiffer designs is less distinct for large PGD.

Figure 6.21 shows the total structural loss separating contours for the four building designs with perfect and brittle welds. The prediction models show that the probability of total structural loss depends on PGD only for ground motions with PGD_{lp} less than 1 m. The six- and twenty-story, more flexible designs with perfect welds would be deemed total structural losses in ground motions with PGV_{lp} greater than approximately 1.5 m/s and 1.2 m/s, respectively. The other considered building models would likely be total structural losses in ground motions with PGV_{lp} greater than 0.5–1 m/s.

Figure 6.22 compares the relative performance of the steel moment frame buildings assuming they are repairable following an earthquake. As expected, the stiffer, higher-strength designs have lower peak IDR compared to the more flexible, lower-strength designs for the same PSA. The six-story designs have lower peak IDR compared to the equivalent twenty-story designs, and the presence of brittle welds increases the expected peak IDR.

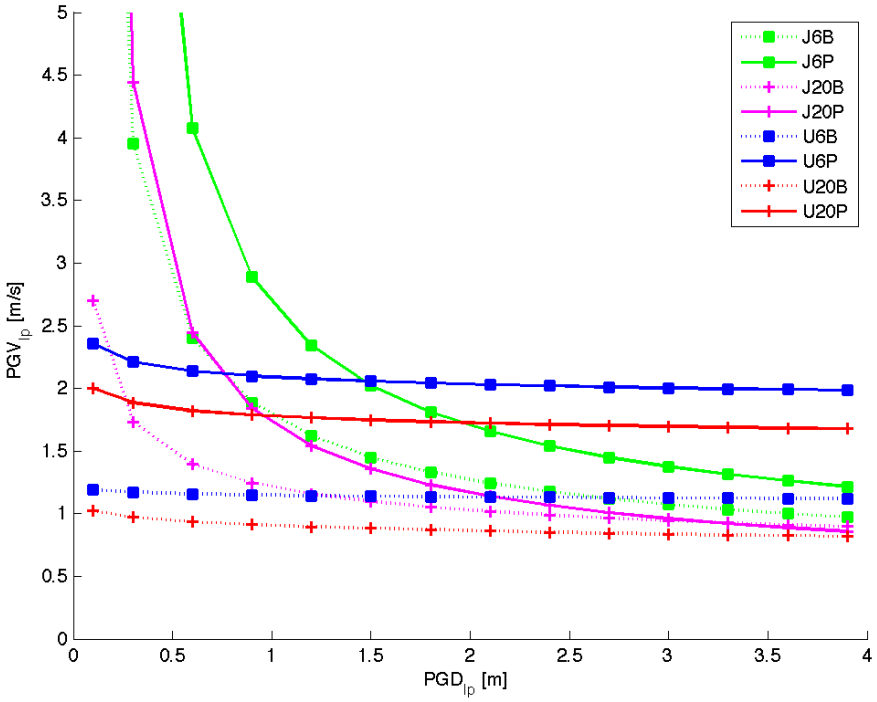

Figure 6.20: This figure shows the collapse separating contours (30% probability of collapse) as functions of peak ground displacement and velocity for the four building designs with brittle or perfect welds. The presence of brittle welds significantly increases the probability of collapse. The stiffness and strength of the building design changes the shape of the separating contour. A six-story building is less likely to collapse in a given ground motion than a twenty-story building.

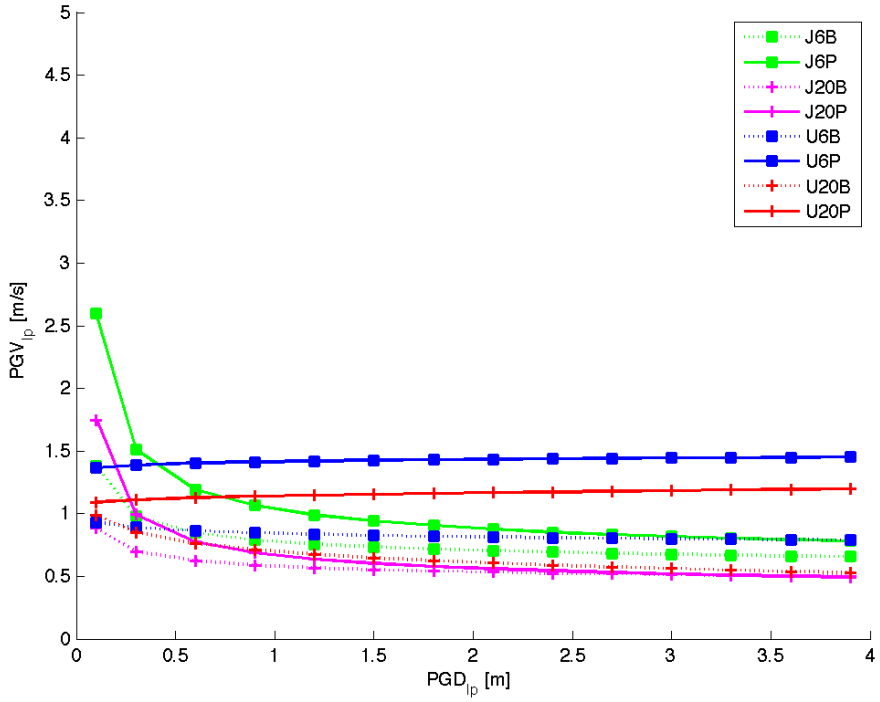

Figure 6.21: This figure shows the total structural loss separating contours (30% probability of total structural loss) as functions of peak ground displacement and velocity. The probability of total structural loss is mostly independent of PGD, and only somewhat dependent on PGV for small PGD. The separating contours of the more flexible, lower-strength designs of twenty and six stories are at approximately 1 and 1.5 m/s, respectively. The separating contours for the other considered designs and for buildings with brittle welds are mostly between 0.5 and 1 m/s.

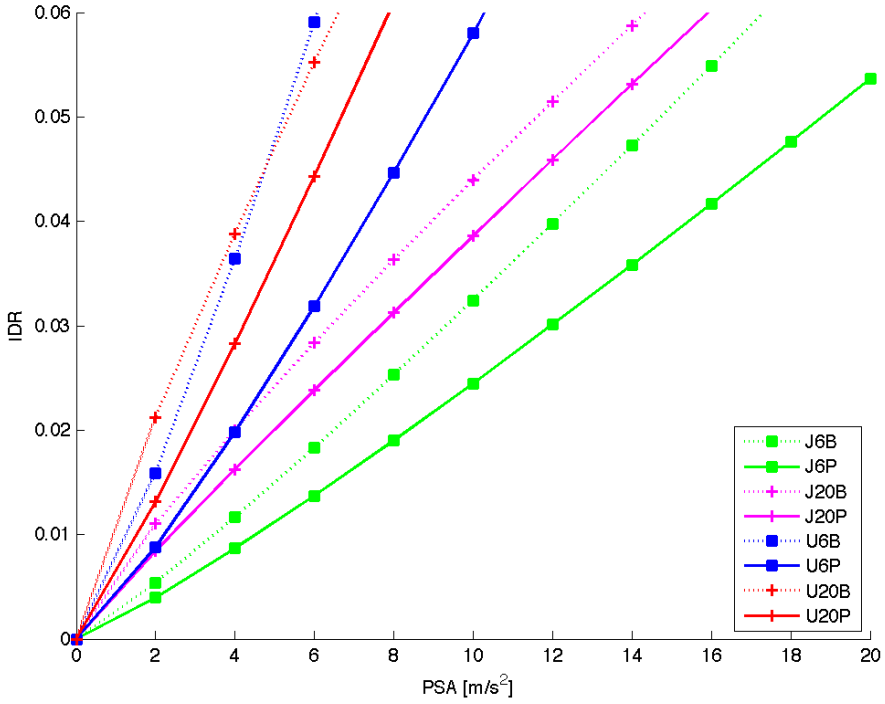

Figure 6.22: Pseudo-spectral acceleration best predicts the peak inter-story drift ratio, assuming that the building is not a total structural loss. The expected peak inter-story drift ratio in buildings with stiffer designs is smaller than the expectation for more flexible designs. Six-story buildings have smaller peak inter-story drifts than the similarly designed twenty-story buildings. The presence of brittle welds increases the expected peak inter-story drift ratio.

Recall that the building response prediction models developed in this chapter are based on simulated data. These prediction models have not been validated against the experiences of steel moment frames in historic earthquakes. Validating these models would require knowing the ground motion—or at least the intensity measure—at each steel moment frame that was subjected to strong ground motions. One result of this thesis is to anticipate the building response in ground motions not previously experienced in modern urban areas. Thus it may not be possible to validate these prediction models with available data from historic earthquakes.